Journal of Computational Physics 257 (2014) 374–399

Contents lists available at ScienceDirect

Journal of Computational Physics

www.elsevier.com/locate/jcp

Combination of topology optimization and optimal control method

Yongbo Deng *, Zhenyu Liu, Yongshun Liu, Yihui Wu

State Key Laboratory of Applied Optics, Changchun Institute of Optics, Fine Mechanics and Physics (CIOMP), Chinese Academy of Sciences, 130033, Changchun, Jilin, China

ARTICLE INFO

Article history:
Received 25 July 2012
Received in revised form 27 August 2013
Accepted 6 September 2013
Available online 9 October 2013

Keywords:
Topology optimization
Optimal control
Optimal match

ABSTRACT

This paper presents the combination of topology optimization and optimal control method to find the optimal match between the material topology and control. In the presented method, the material topology is determined using the SIMP (Solid Isotropic Material with Penalization) method, which has been popularly used in topology optimization. In the SIMP method, the design variable is relaxed and bounded in the interval $[0, 1]$, and the evolution of the design variable is usually implemented by the method of moving asymptotes (MMA), which can be used to deal with optimization problem with multiple integral constraints and bound constraint of the design variable. In the combination of topology optimization and optimal control method, the control variable appears along with the design variable. In order to evolve the control variable and design variable using MMA simultaneously, the control variable is regularized using a bound constraint and the corresponding bound constraint is projected onto the interval $[0, 1]$, which is the same as the bound constraint of the design variable. The optimization problem is analyzed using the adjoint method to obtain the adjoint sensitivity. During the optimization procedure, the design and control variables are filtered by the Helmholtz filters to ensure the smoothness of the distribution. To ensure the minimum scale length and remove the gray area in the material topology, the filtered design variable is projected by the threshold method. The feasibility and robustness of the combination of these two methods are demonstrated by several test problems, including heat transfer, fluid flow and compliance minimization.

1. Introduction

In topology optimization, the optimal topology of materials is computed under the given control. At the same time, the optimal control is calculated under the fixed material layout in optimal control method. Naturally, one has the question that is how to find the optimal match of the material topology and control to present the reasonable designs of the material layout and control simultaneously. Therefore, this paper is focused on the combination of topology optimization and optimal control method to find the optimal match between the material topology and control. Based on the combination of topology optimization and optimal control method, the layout and control of a device can be optimized simultaneously, and the freedom of the engineering design can also be enlarged.

Layout optimization and optimal control method have been interesting fields with respect to theory and application for several decades [1–5]. The goal of layout optimization is to achieve better performance for a user specified objective. Usually, layout optimization is categorized into shape optimization and topology optimization. Shape optimization improves the performance of a device by adjusting the positions of structural boundaries, keeping the topology of the structure unchanged.

* Corresponding author.
E-mail addresses: dengyb@ciomp.ac.cn (Y. Deng), yihuiwu@ciomp.ac.cn (Y. Wu).

0021-9991/$ – see front matter
http://dx.doi.org/10.1016/j.jcp.2013.09.033

Topology optimization is a method used to determine the optimal distribution of materials. Topology optimization can optimize the shape and topology, simultaneously. Therefore, topology optimization is a more general optimization technique than shape optimization. Currently, the topology optimization is mainly implemented using the SIMP method [6–8] and the level set method [9–12]. Topology optimization based on the SIMP method was first used to design stiffness and compliance mechanisms [7,13–17] and has been extended to multiple physical problems, such as acoustic, electromagnetic, fluidic, optical and thermal problems [18–23,25]. The level set method, pioneered by Osher and Sethian [26], accomplishes the change of topology by evolving and merging the zero contours of the level set function. This method provides a general way to track the implicit interface between two phases, and it has been applied to shape and topology optimization [27,28]. One of the major advantages of the level set method lies in expressing continuously moving interfaces and abstracting the material domains that correspond to the structural topology. Recently, it has been observed that the conventional level set method may be inadequate for the cases in which the initial shape of the structure has fewer holes than the optimal geometry [10], especially in two-dimensional cases. The above difficulty can be overcome using topological sensitivity, which was introduced by Sokolowski and Zochowski [29] for linear elasticity and has been extended to several other linear and nonlinear physical problems [30–33]. Comparing with the level set method, the SIMP method has the merits on rapid and robust convergency, weak dependence on the initial distribution of the design variable, and dealing with multiple constraints. Therefore, the SIMP method is chosen to perform the topology optimization in this paper. On the other hand, the optimal control method has numerous applications spanning many branches of engineering science, such as internal combustion engines, airbreathing engines, heat exchangers, control of heat rejection devices in computers, flow control problems in ink jet printers, manufacturing problems in microelectronic chips, control of pollutant transport, control of metal forming, control of chemical reactors, control of aerodynamic surfaces, and weather prediction [34]. For many years, optimal control has been an ad-hoc subject in engineering science despite its importance. Advances in high-performance computing of three-dimensional time dependent problems and recent developments in nonlinear infinite-dimensional systems theory and nonlinear partial differential equations have set the stage for optimal control theory. The subject has been under rapid development since the early works in [3–5,35–39]. The impact of this development to continuum mechanics has been essentially in the branch of solid mechanics. Several theorems relating the Navier–Stokes equations and the minimization of certain functionals were established in [40–44], thus starting the optimal control method in fluid mechanics.

Because the optimal control problem includes two types, i.e. the optimal distribution control and optimal boundary control, the combination discussed in this paper can be respectively categorized into the combination of topology optimization with optimal distribution control and optimal boundary control. This paper is organized as follows: the abstract form of the variational problem and the adjoint analysis are stated in Section 2 for the combination method; the numerical implementation on solving the corresponding variational problem are presented in Section 3; several test problems are presented in Section 4 to demonstrate the feasibility and robustness of the combination method; and the paper is concluded in Section 5. In the following, all the mathematical descriptions are performed in the Cartesian coordinate system.

2. Methodology

2.1. Variational problem and regularization

The variational problem for the combination of topology optimization and optimal control method are typical optimization problem constrained by partial differential equations, and it can be written in the following abstract form:

$$\begin{aligned} &\text{Find:} \quad (\gamma, u) \\ &\text{Min:} \quad J(y;\gamma,u) \\ &\text{S.t.} \quad e(y;\gamma,u)=0; \quad \gamma\in\mathcal{K}_\gamma,\ u\in\mathcal{K}_u \end{aligned} \tag{1}$$

where $y\in \mathrm{Y}$ is the state variable which can be a scalar or vector; $\gamma\in \mathrm{V}$ is the design variable; $u\in \mathrm{U}$ is the control variable; y, γ and u are functionals defined on the open and bounded domain Ω with Lipschitz boundary; $\mathcal{K}_\gamma\subset \mathrm{V}$ and $\mathcal{K}_u\subset \mathrm{U}$ are sets of the feasible values of γ and u; $J:\mathrm{Y}\times\mathrm{V}\times\mathrm{U}\to\mathbb{R}$ and $e:\mathrm{Y}\times\mathrm{V}\times\mathrm{U}\to\mathrm{Z}$ are bounded continuous mapping operator; Y, V, U and Z are Banach spaces; $\mathcal{K}_\gamma$ and $\mathcal{K}_u$ are convex sets. A quite common situation is that $e:\mathrm{Y}\times\mathrm{V}\times\mathrm{U}\to Z$ is continuously Fréchet differentiable and $e_y(y;\gamma,u)\in\mathcal{L}(\mathrm{Y},Z)$ has the bounded inverse. Then according to the implicit function theorem [46], the partial differential equation $e(y;\gamma,u)=0$ locally defines a continuously Fréchet differentiable map $(\gamma,u)\mapsto y(\gamma,u)$, which has the following Fréchet derivative:

$$y'(\gamma,u)=-e_y^{-1}(y;\gamma,u)e_{(\gamma,u)}(y;\gamma,u) \tag{2}$$

Therefore, the optimization problem in Eqs. (1) is transformed into

$$\text{Min:} \quad \hat{J}(\gamma,u)=J\big(y(\gamma,u);\gamma,u\big); \quad \gamma\in\mathcal{K}_\gamma,\ u\in\mathcal{K}_u \tag{3}$$

In topology optimization based on the SIMP method, the design variable is relaxed and bounded in a given interval, typically $[0,1]$, where the values 0 and 1 represent two different materials respectively. Then the set of the feasible values of the design variable in Eq. (1) is $\mathcal{K}_\gamma=[0,1]$. Based on the gradient information of the optimization problem, the design

variable is penalized and evolved to the value 0 or 1 at a fixed point in the design domain. Currently, the evolution of the design variable in the SIMP optimization is usually achieved using the method of moving asymptotes (MMA) [45], which can be used to deal with the optimization problem with multiple integral constraints and bound constraint of the design variable. In the combination of topology optimization and optimal control method, the control variable appears along with the design variable. In order to evolve the control and design variables using MMA simultaneously, the control variable is regularized using a bound constraint and the bound constraint is projected onto the interval $[0, 1]$, which is the same as the bound constraint of the design variable in topology optimization. The bound constraint of the control variable is

$$u_l \leqslant u \leqslant u_h \tag{4}$$

where u_l and u_h are the lower and upper bounds of the control variable, and the bounds can be determined based on the engineering requirement. Then the feasible set of the control variable in Eq. (1) is $\mathcal{K}_u = [u_l, u_h]$. The projection of the bound constraint of the control variable is carried out using the following substitution:

$$u(u_{01}) = u_l + u_{01}(u_h - u_l), \quad u_{01} \in [0, 1] \tag{5}$$

where u_{01} is the projected control variable. Because the mapping between u_{10} and u is continuous and linear, u_{10} satisfies $u_{10} \in \mathrm{U}$. By Eq. (5), the bound constraint of the control variable $u \in [u_l, u_h]$ is projected onto $u_{01} \in [0, 1]$.

Based on the above regularization, the optimization problem in Eq. (3) can be transformed furthermore:

$$\text{Min:} \quad \hat{J}\big(\gamma, u(u_{01})\big) = J\big(y\big(\gamma, u(u_{01})\big); \gamma, u(u_{01})\big); \quad \gamma \in [0, 1],\ u_{01} \in [0, 1] \tag{6}$$

The gradient information of γ and u_{10} in Eq. (6) can be obtained after the adjoint analysis. Based on the gradient information, the variational problem for the combination of topology optimization and optimal control method can be solved using iterative approach.

2.2. Adjoint analysis

In this section, the variational problem is analyzed to obtain the gradient information. According to [47–49], the adjoint method is an efficient approach to derive the derivative of the objective in the partial differential equation constrained optimization problem. From the Gâteaux derivative of $\hat{J}$, one can obtain

$$\begin{aligned}
\big\langle \hat{J}', s\big\rangle_{(\mathrm{V}\times\mathrm{U})^*,\mathrm{V}\times\mathrm{U}} &= \big\langle J_y, y's\big\rangle_{\mathrm{Y}^*,\mathrm{Y}} + \big\langle (J_\gamma, J_u u_{u_{10}}), s\big\rangle_{(\mathrm{V}\times\mathrm{U})^*,\mathrm{V}\times\mathrm{U}} \\
&= \big\langle y'^* J_y, s\big\rangle_{(\mathrm{V}\times\mathrm{U})^*,\mathrm{V}\times\mathrm{U}} + \big\langle (J_\gamma, J_u u_{u_{10}}), s\big\rangle_{(\mathrm{V}\times\mathrm{U})^*,\mathrm{V}\times\mathrm{U}} \\
&= \big\langle y'^* J_y + (J_\gamma, J_u u_{u_{10}}), s\big\rangle_{(\mathrm{V}\times\mathrm{U})^*,\mathrm{V}\times\mathrm{U}} \\
&= \big\langle (e_\gamma, e_u u_{u_{10}})^* \big(-e_y^{-1}\big)^* J_y + (J_\gamma, J_u u_{u_{10}}), s\big\rangle_{(\mathrm{V}\times\mathrm{U})^*,\mathrm{V}\times\mathrm{U}}; \quad \forall s \in \mathrm{V}\times\mathrm{U}
\end{aligned} \tag{7}$$

where $(\cdot)^*$ is the adjoint operator of $(\cdot)$; $\langle\cdot,\cdot\rangle$ represents the dual pairing of $(\mathrm{V}\times\mathrm{U})^*$ and $\mathrm{V}\times\mathrm{U}$. By setting

$$\lambda = \big(-e_y^{-1}\big)^* J_y = -\big(e_y^*\big)^{-1} J_y \tag{8}$$

one can obtain

$$\big\langle e_y^* \lambda, v\big\rangle_{\mathrm{Y}^*,\mathrm{Y}} = \langle -J_y, v\rangle_{\mathrm{Y}^*,\mathrm{Y}}, \quad \forall v \in \mathrm{Y} \tag{9}$$

where $\lambda \in Z^*$ is the adjoint variable of y; e_y^* is the adjoint operator of e_y. And the Gâteaux derivative of $\hat{J}$ can be reduced to be:

$$\big\langle \hat{J}', s\big\rangle_{(\mathrm{V}\times\mathrm{U})^*,\mathrm{V}\times\mathrm{U}} = \big\langle (e_\gamma, e_u u_{u_{10}})^* \lambda + (J_\gamma, J_u u_{u_{10}}), s\big\rangle_{(\mathrm{V}\times\mathrm{U})^*,\mathrm{V}\times\mathrm{U}}, \quad \forall s \in \mathrm{V}\times\mathrm{U} \tag{10}$$

If $\hat{J}$ is Fréchet differentiable, the adjoint equation

$$e_y^* \lambda = -J_y \tag{11}$$

and the adjoint derivative

$$\hat{J}' = (e_\gamma, e_u u_{u_{10}})^* \lambda + (J_\gamma, J_u u_{u_{10}}) \tag{12}$$

can be obtained. According to the Kurash–Kuhn–Tucker condition [47], the solution of the variational problem in Eq. (1) satisfies the following system:

Table 1
Procedure of the iterative approach.

1.	Give the initial values of the design and control variables;
2.	Solve the partial differential equations;
3.	Solve the adjoint equations; compute the adjoint derivatives and corresponding objective and integral constraint values;
4.	Update the design and control variables using MMA;
5.	Check for convergence; if the stopping conditions are not satisfied, go to 2;
6.	Post processing

$$
\begin{aligned}
&e\big(y;\gamma,u(u_{10})\big)=0\\
&e_y^*\lambda=-J_y\\
&\frac{DJ}{D\gamma}=e_\gamma^*\lambda+J_\gamma\begin{cases}=0, & \text{if } 0<\gamma<1\\ \geqslant 0, & \text{if } \gamma=0\\ \leqslant 0, & \text{if } \gamma=1\end{cases}\\
&\frac{DJ}{Du_{10}}=(e_u u_{u_{10}})^*\lambda+J_u u_{u_{10}}\begin{cases}=0, & \text{if } 0<u_{10}<1\\ \geqslant 0, & \text{if } u_{10}=0\\ \leqslant 0, & \text{if } u_{10}=1\end{cases}
\end{aligned}
\tag{13}
$$

In engineering, the variational problem may need to be regularized furthermore by some integral constraints, e.g. volume constraint. The adjoint analysis of these integral constraints is the same as that for the objective. The equation system in Eq. (13) usually has strong nonlinearity and it is difficult to solve the system directly. Therefore, the iterative approach is widely adopted. In the iterative approach, the descent direction can be defined based on the adjoint derivative, where the state and adjoint variables are obtained by solving the partial differential equations and corresponding adjoint equations respectively.

3. Numerical implementation

After the adjoint analysis, the variational problem for the combination of topology optimization and optimal control method can be solved using the iterative approach based on the gradient information. The procedure for the iterative approach includes the following steps (Table 1): (a) the partial differential equations are solved with the given values of the design and control variables; (b) the adjoint equations are solved based on the numerical solution of the partial differential equations; (c) the adjoint derivatives of the objective functional and integral constraint are computed; (d) the design and control variables are updated using MMA. The above steps are implemented iteratively until the stopping criteria are satisfied. In this paper, the stopping criteria are specified as the change of the objective values in 5 consecutive iterations satisfying

$$
\sum_{i=0}^{4}|J_{k-i}-J_{k-i-1}|/|J_k|<\epsilon \tag{14}
$$

in the k-th iteration, where J_k and γ_k are the objective value and the distribution of the design variable in the k-th iteration, respectively; ϵ is the tolerance chosen to be 1×10^{-3}. The maximal iterative number is chosen to be 400. If there is an integral constraint, the relative residual of the integral constraint is required to be less than 1×10^{-3} when the iterative procedure converges. In the above iterative procedure, the partial differential equations and corresponding adjoint equations are solved by the finite element method using the commercial finite element software *COMSOL Multiphysics* (Version 3.5) [50], where all the numerical implementation are based on the software's basic module: *Comsol Multiphysics* → *PDE Modes* → *PDE, General Form*. For the details on the setting of the *PDE Modes* and the numerical integrations in the optimization procedure, one can refer to [51,52].

During the optimization procedure, the design and control variables are filtered by the Helmholtz filters [53,54] to ensure the distribution smoothness, where the Helmholtz filters are implemented by solving the following Helmholtz equations:

$$
\begin{aligned}
&-r^2\nabla\cdot\nabla\widetilde{\gamma}+\widetilde{\gamma}=\gamma, \quad \text{in } \Omega\\
&\nabla\widetilde{\gamma}\cdot\mathbf{n}=0, \quad \text{on } \partial\Omega
\end{aligned}
\tag{15}
$$

$$
\begin{aligned}
&-r^2\nabla\cdot\nabla\widetilde{u}+\widetilde{u}=u, \quad \text{in } \Omega\\
&\nabla\widetilde{u}\cdot\mathbf{n}=0, \quad \text{on } \partial\Omega
\end{aligned}
\tag{16}
$$

where r is the filter radius chosen based on numerical experiments [54]; $\widetilde{\gamma}$ and $\widetilde{u}$ are the filtered design and control variables, respectively. The filtered control variable $\widetilde{u}$ is called physical control in this paper. To ensure the minimum scale

length and remove the gray area in the obtained material topology, the filtered design variable is projected by the threshold method [55–57]:

$$\overline{\widetilde{\gamma}}(\widetilde{\gamma}) = \frac{\tanh(\beta\xi) + \tanh(\beta(\widetilde{\gamma} - \xi))}{\tanh(\beta\xi) + \tanh(\beta(1 - \xi))} \tag{17}$$

where $\overline{\widetilde{\gamma}}$ is the projected design variable called physical density representing the material topology [57]; $\xi \in [0, 1]$ and β are the threshold and projection parameters for the threshold projection, respectively. On the choice of the values of ξ and β, one can refer to [55,58]. Because the design and control variables are filtered by Helmholtz filters, the Helmholtz equations are included in the partial differential equation constraints of the variational problem (Eq. (1)). Then $\widetilde{\gamma}$ and $\widetilde{u}$ are regarded as two of the components of the state vector y. And the adjoint equations of the Helmholtz equations are included in the adjoint equations.

In the following, the combination of topology optimization and optimal distribution control method is presented in Section 4.1; the combination of topology optimization and optimal boundary control method is demonstrated in Section 4.2; the combination of topology optimization and optimal control method is exhibited for the transient problem in Section 4.3. Several problems are defined and tested to verify the feasibility and robustness of the combination of topology optimization and optimal control method. The test problems include the heat transfer, fluid flow and compliance minimization. In these test problems, the partial differential equations are solved using the standard Galerkin finite element method. In the heat transfer problem, the temperature and its adjoint variable are interpolated quadratically; in the fluid flow problem, the Navier–Stokes equations and corresponding adjoint equations are solved using Taylor–Hood elements [59], where the fluid velocity and its adjoint are interpolated quadratically, and the pressure and its adjoint are interpolated linearly; in the compliance minimization, the displacement and its adjoint are interpolated quadratically; in the Helmholtz filters, the filtered design variable, filtered control variable and the corresponding adjoint variables are solved using linear elements; in addition, the design and control variables are interpolated linearly. All the computation are performed on a DELL workstation (DELL PRECISION T5500, two Intel Xeon Quad X5550 CPUs).

4. Test problems

4.1. Combination of topology optimization and optimal distribution control

4.1.1. Heat transfer

The heat transfer problem has been investigated using the topology optimization method [24,25,60,61] and optimal control method [62] respectively, where the heat source is fixed in topology optimization and the layout of the heat conductive materials are fixed in optimal control. Based on the intuition, one can conclude that a reasonable match between the layout of the heat conductive materials and the distribution of the heat source can be more effective. Then the combination of topology optimization and optimal distribution control is used to achieve this by solving the following variational problem:

$$\begin{aligned}
&\text{Find:} \quad (\gamma, Q)\\
&\text{Min:} \quad J(T;\gamma,Q) = \int_{\Omega} \omega_1 A(T, \nabla T; \overline{\widetilde{\gamma}}, \widetilde{Q})\,\mathrm{d}\Omega + \int_{\partial\Omega} \omega_2 B(T; \overline{\widetilde{\gamma}}, \widetilde{Q})\,\mathrm{d}\Gamma\\
&\text{S.t.} \quad \begin{cases}
\begin{cases} \nabla\cdot(-k\nabla T) = \widetilde{Q}, & \text{in } \Omega \\ T = T_D, & \text{on } \Gamma_D \\ k\nabla T\cdot\mathbf{n} = g, & \text{on } \Gamma_N \end{cases} & \text{(Heat transfer)}\\
\begin{cases} -r^2\nabla\cdot\nabla\widetilde{\gamma} + \widetilde{\gamma} = \gamma, & \text{in } \Omega \\ \nabla\widetilde{\gamma}\cdot\mathbf{n} = 0, & \text{on } \partial\Omega \end{cases} & \text{(Filter of } \gamma)\\
\begin{cases} -r^2\nabla\cdot\nabla\widetilde{Q} + \widetilde{Q} = Q, & \text{in } \Omega \\ \nabla\widetilde{Q}\cdot\mathbf{n} = 0, & \text{on } \partial\Omega \end{cases} & \text{(Filter of } Q)\\
\int_{\Omega} \overline{\widetilde{\gamma}}\,\mathrm{d}\Omega \leqslant \theta_{Vol} V_0 & \text{(Volume constraint)}\\
0 \leqslant \gamma \leqslant 1 & \text{(Bound of } \gamma)\\
Q_l(\mathbf{x}) \leqslant Q \leqslant Q_h(\mathbf{x}), \quad \mathbf{x}\in\Omega & \text{(Bound of } Q)
\end{cases}
\end{aligned} \tag{18}$$

where T is the temperature; k is the thermal conductivity; T_D is the known temperature on the boundary Γ_D; g is the heat flux on the boundary Γ_N, which is the insulative boundary as $g = 0$; Ω is the design domain; ω_1 and ω_2 are the weights of the two integrations of A and B in the objective; Q_l and Q_h, chosen based on the engineering requirement, are the lower and upper bounds of the control variable Q, respectively; the design variable γ and control variable Q are filtered by the Helmholtz filters; $\widetilde{\gamma}$ and $\widetilde{Q}$ are the filtered design variable and filtered control variable, respectively; the filtered control variable $\widetilde{Q}$ is called physical control representing the heating source; $\overline{\widetilde{\gamma}}$ is the projected design variable (Eq. (17)); the

optimization problem is regularized by a volume constraint; θ_{Vol} is the upper bound of the volume fraction of the thermal conductive material; V_0 is the volume of the design domain Ω. In the above described variational problem, the control variable Q corresponds to the variable u in Eq. (1); the temperature T, the filtered variables $\widetilde{\gamma}$ and $\widetilde{Q}$ correspond to the components of the state vector y in Eq. (1).

In the above variational problem (Eq. (18)), the material interpolation of the thermal conductivity k is the same as that in the topology optimization of heat transfer problem [24]:

$$k(\overline{\widetilde{\gamma}}) = k_{min} + (k_{max} - k_{min})\overline{\widetilde{\gamma}}^m \tag{19}$$

where k_{min} and k_{max} are the thermal conductivity of the thermal insulative and conductive materials, respectively; m is the penalty, chosen to be 3. The bound constraint of the control variable is projected onto [0, 1] using the following substitution:

$$Q = Q_l + Q_{01}(Q_h - Q_l), \quad Q_{01} \in [0,1] \tag{20}$$

where Q_{01} is the projected control variable. When the iterative procedure is converged, the physical density $\overline{\widetilde{\gamma}}$ and physical control $\widetilde{Q}$ can be obtained based on the obtained distributions of γ and Q_{01}, respectively.

The analysis of the variational problem in Eq. (18) can be implemented based on the adjoint method in Section 2.2. Then the adjoint equation of the heat transfer equation is obtained as:

$$\begin{aligned}
&\nabla\cdot(-k\nabla T_a) = -\omega_1\left(\frac{\partial A}{\partial T} - \nabla\cdot\frac{\partial A}{\partial \nabla T}\right), \quad \text{in } \Omega\\
&T_a = 0, \quad \text{on } \Gamma_D\\
&k\nabla T_a\cdot\mathbf{n} = -\left(\omega_1\frac{\partial A}{\partial \nabla T}\cdot\mathbf{n} + \omega_2\frac{\partial B}{\partial T}\right), \quad \text{on } \Gamma_N
\end{aligned} \tag{21}$$

where T_a is the adjoint variable of T. The adjoint equations of the Helmholtz filters for the design and control variables are obtained as:

$$\begin{aligned}
&-r^2\nabla\cdot\nabla\widetilde{\gamma}_a + \widetilde{\gamma}_a = -\left(\omega_1\frac{\partial A}{\partial\overline{\widetilde{\gamma}}} + \frac{\partial k}{\partial\overline{\widetilde{\gamma}}}\nabla T\cdot\nabla T_a\right)\frac{\partial\overline{\widetilde{\gamma}}}{\partial\widetilde{\gamma}}, \quad \text{in } \Omega\\
&r^2\nabla\widetilde{\gamma}_a\cdot\mathbf{n} = -\omega_2\frac{\partial B}{\partial\overline{\widetilde{\gamma}}}\frac{\partial\overline{\widetilde{\gamma}}}{\partial\widetilde{\gamma}}, \quad \text{on } \partial\Omega
\end{aligned} \tag{22}$$

$$\begin{aligned}
&-r^2\nabla\cdot\nabla\widetilde{Q}_a + \widetilde{Q}_a = -\omega_1\frac{\partial A}{\partial\widetilde{Q}} + T_a, \quad \text{in } \Omega\\
&r^2\nabla\widetilde{Q}_a\cdot\mathbf{n} = -\omega_2\frac{\partial B}{\partial\widetilde{Q}}, \quad \text{on } \partial\Omega
\end{aligned} \tag{23}$$

where $\widetilde{\gamma}_a$ and $\widetilde{Q}_a$ are the adjoint variables of $\widetilde{\gamma}$ and $\widetilde{Q}$, respectively. And the adjoint derivatives are obtained as:

$$\begin{aligned}
&\left.\frac{DJ}{D\gamma}\right|_\Omega = -\widetilde{\gamma}_a\\
&\left.\frac{DJ}{DQ_{01}}\right|_\Omega = -\widetilde{Q}_a\frac{\partial Q}{\partial Q_{01}}
\end{aligned} \tag{24}$$

It is valuable to notice that the partial differential equations and their corresponding adjoint equations have the same global stiffness matrix, when the finite element method is used. Therefore, the corresponding global stiffness matrix needs to be assembled only once in the whole iterative procedure.

One numerical example is presented to demonstrate the combination of topology optimization and optimal distribution control for the heat transfer problem. By setting the design domain as shown in Fig. 1(a), the thermal compliance as the objective with $A = k\nabla T\cdot\nabla T$ and $B = 0$, and the parameters as listed in Table 2, the variational problem is solved, where the design domain is discretized by 200×200 rectangular elements. The projection parameter β with the initial value 1 is doubled every 40 iterations before reaching the maximum value 1024, and the same method for updating β is used in the following numerical examples. The intention of these setting is to find the optimal match of the material topology and distribution of the heating source to minimize the thermal compliance. The obtained material topology, distribution of the heating source and the corresponding distribution of the temperature are shown in Figs. 1(b), 1(c) and 1(d), respectively. The convergent histories of the objective values and volume fraction are plotted in Fig. 2. Snapshots for the evolution of the material topology and distribution of the heating source during the iterative procedure are plotted in Figs. 3 and 4, respectively.

The material topology in Fig. 3 has the multi-branch shape which increases the area of the interface between the thermal conductive and insulative materials. From the distribution of the heating source and temperature in Figs. 1(c) and 1(d), one can see that the region with low temperature corresponds to higher power of heating source, and the power of heating

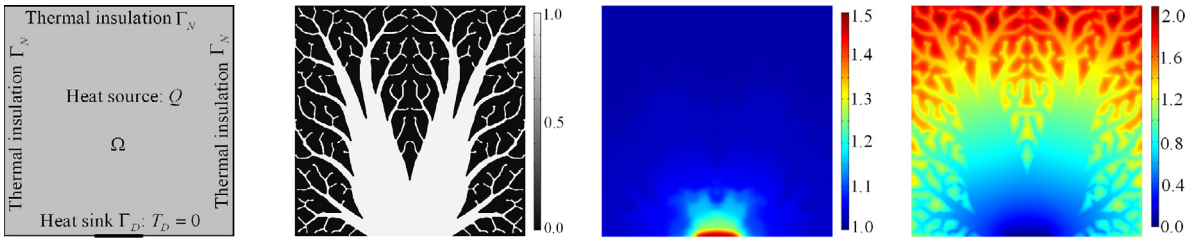

(a) Design domain (b) Material topology (c) Heating source distribution (d) Temperature

Fig. 1. (a) Design domain of the heat transfer problem, where the size is 1×1; (b) material topology of the optimal match; (c) heating source distribution of the optimal match; (d) distribution of the temperature corresponding to the optimal match.

Table 2
Parameter setting for solving the variational problem of heat transfer.

T_D	r	θ_{Vol}	m	k_{min}	k_{max}	ξ	ω_1	ω_2	Q_l	Q_h
0	1×10^{-2}	0.4	3	1×10^{-3}	1×10^{0}	0.5	1	0	1	2

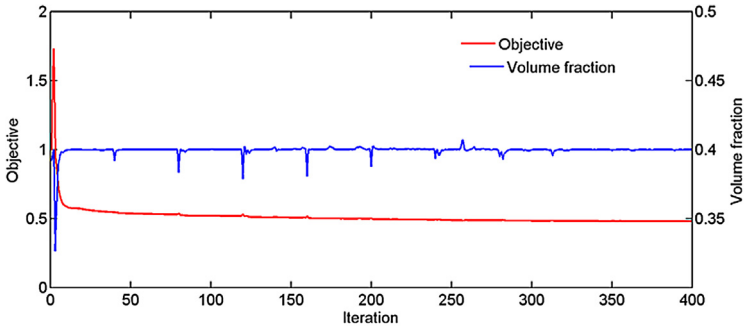

Fig. 2. Convergent histories of the objective values and volume constraint, where the objective values are normalized by the objective value corresponding to the initial distribution of γ and Q. The cost of CPU time is 5.01 h.

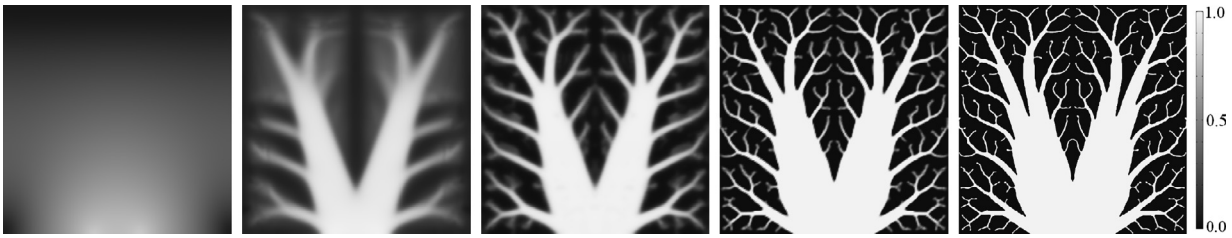

(a) Iteration 1 (b) Iteration 20 (c) Iteration 100 (d) Iteration 220 (e) Iteration 360

Fig. 3. Snapshots for the evolution of the material topology.

source in the conductive material is higher than that in the insulative material. This is propitious to descend the temperature gradient and decrease the thermal compliance.

By fixing the heating source distribution as shown in Fig. 1(c), the corresponding optimal material topology shown in Fig. 5(a) is computed using the topology optimization method. On the other hand, the optimal distribution of the heating source is computed (Fig. 5(b)) by fixing the material topology as shown in Fig. 1(b). The objective values corresponding to Figs. 1(b), 5(a) and 5(b) are listed in Table 3. From the consistency of the values in Table 3, the optimality is confirmed for the obtained match between the material topology and heating source distribution. In order to demonstrate the necessity of the combination method furthermore, the material topology is computed with the heating source distribution set as the constant equal to the lower bond 1 (Fig. 6). And the thermal compliance corresponding to the material topology with constant heating source is 1.3890. Compared with the results shown in Fig. 1, the thermal compliance is decreased up to 18% by the combination method. Therefore, the necessity of the combination method can be confirmed.

To confirm the optimality of the obtained match between the material topology and distribution control, the volume constraint of the distribution is added to the optimization problem as

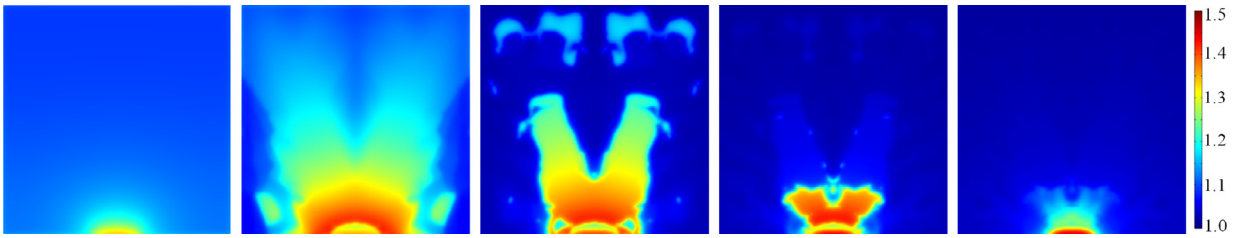

Fig. 4. Snapshots for the evolution of the heating source distribution.

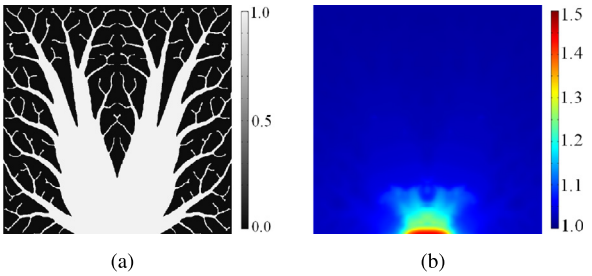

Fig. 5. (a) Optimal material topology computed by fixing the heating source distribution as shown in Fig. 1(c); (b) optimal heating source distribution computed by fixing the material topology as shown in Fig. 1(b).

Table 3
Objective values corresponding to Figs. 1(b), 5(a) and 5(b).

Fig. 1(b)	Fig. 5(a)	Fig. 5(b)
1.1456	1.1477	1.1409

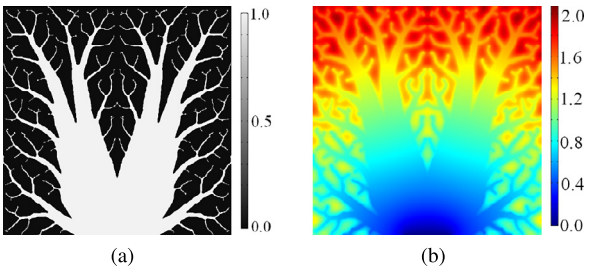

Fig. 6. (a) Optimal material topology computed by setting the heating source distribution as the constant equal to the lower bond 1; (b) distribution of the temperature corresponding to the optimal material topology. The corresponding objective value is 1.3890. Compared with the results shown in Fig. 1, the combination method decreases the thermal compliance up to 18%.

Table 4
Objective values corresponding to different volume fractions of the distribution control.

$\theta_{\widetilde{Q}} = 0.50$	$\theta_{\widetilde{Q}} = 0.52$	$\theta_{\widetilde{Q}} = 0.54$	$\theta_{\widetilde{Q}} = 0.56$	$\theta_{\widetilde{Q}} = 0.58$	$\theta_{\widetilde{Q}} = 0.60$
1.1842	1.1452	1.2023	1.2823	1.2946	1.3169

$$\int_{\Omega} \widetilde{Q}\, d\Omega = \theta_{\widetilde{Q}} V_{Q0} \tag{25}$$

where $\theta_{\widetilde{Q}}$ is the volume fraction of the physical control; $V_{Q0} = \int_{\Omega} Q_h\, d\Omega$. For different volume fraction of the physical control, the optimization is solved and the corresponding objective values are listed in Table 4. The optimal match in Fig. 1 corresponds to the volume fraction $\theta_{\widetilde{Q}} = 0.52$. Then based on the objective values listed in Table 4, the optimality of the match between the material topology and distribution control, obtained by solving the optimization Problem (18), can be confirmed furthermore.

4.1.2. Fluid flow

In this section, the combination of topology optimization and optimal distribution control method is tested for the fluid flow problem. The flow of the Newtonian fluid is described by the Navier–Stokes equations widely [63]. Topology optimization using the SIMP method for fluid problems was first researched for Stokes flows [19,64,65] and Darcy–Stokes flows [66,67]. It was later extended to Navier–Stokes flows [27,28,51,68,69] and non-Newtonian flows [70]. Additionally, the topology optimization method has been applied to design fluid devices [71–76]. In the topology optimization of fluid flow, the artificial Darcy force is added to the Navier–Stokes equations, where the solid and fluid phases are approximated by the porous media with high and low impermeability respectively [19]. In the optimal distribution control of the fluid flow, the control variable is the distribution of the body force in a specified domain, and this has been investigated for several engineering applications, i.e. velocity tracking problem [77,78]. At the same time, the better match between the topology of the fluid domain and distribution control can be more effective for achieving the desired performance of the fluid flow. Therefore, the following variational problem is constructed for the fluid flow to find the optimal match:

$$
\begin{aligned}
&\text{Find:} \quad (\gamma, \mathbf{f})\\
&\text{Min:} \quad J(\mathbf{u}, p; \gamma, \mathbf{f}) = \int_{\Omega} \omega_1 A(\mathbf{u}, \nabla\mathbf{u}, p; \widetilde{\overline{\gamma}}, \widetilde{\mathbf{f}})\,\mathrm{d}\Omega + \int_{\partial\Omega} \omega_2 B(\mathbf{u}, p; \widetilde{\overline{\gamma}}, \widetilde{\mathbf{f}})\,\mathrm{d}\Gamma\\
&\text{S.t.} \quad \begin{cases}
\begin{cases}
\rho\mathbf{u}\cdot\nabla\mathbf{u} - \nabla\cdot\left[\eta\left(\nabla\mathbf{u} + \nabla\mathbf{u}^{\mathrm{T}}\right)\right] + \nabla p = -\alpha\mathbf{u} + \widetilde{\mathbf{f}}\widetilde{\overline{\gamma}}^{m}, & \text{in } \Omega\\
-\nabla\cdot\mathbf{u} = 0, & \text{in } \Omega\\
\mathbf{u} = \mathbf{u}_D, & \text{on } \Gamma_D\\
\left[p\mathbf{I} - \eta\left(\nabla\mathbf{u} + \nabla\mathbf{u}^{\mathrm{T}}\right)\right]\cdot\mathbf{n} = \mathbf{g}, & \text{on } \Gamma_N
\end{cases} \quad \text{(Navier–Stokes equations)}\\
\begin{cases}
-r^2\nabla\cdot\nabla\widetilde{\gamma} + \widetilde{\gamma} = \gamma, & \text{in } \Omega\\
\nabla\widetilde{\gamma}\cdot\mathbf{n} = 0, & \text{on } \partial\Omega
\end{cases} \quad \text{(Filter of } \gamma\text{)}\\
\begin{cases}
-r^2\nabla\cdot\nabla\widetilde{\mathbf{f}} + \widetilde{\mathbf{f}} = \mathbf{f}, & \text{in } \Omega\\
\nabla\widetilde{\mathbf{f}}\cdot\mathbf{n} = \mathbf{0}, & \text{on } \partial\Omega
\end{cases} \quad \text{(Filter of } \mathbf{f}\text{)}\\
\int_{\Omega} \widetilde{\overline{\gamma}}\,\mathrm{d}\Omega \leqslant \theta_{Vol} V_0 \quad \text{(Volume constraint)}\\
0 \leqslant \gamma \leqslant 1 \quad \text{(Bound of } \gamma\text{)}\\
f_{li}(\mathbf{x}) \leqslant f_i \leqslant f_{hi}(\mathbf{x}), \quad \mathbf{x}\in\Omega,\ i = 1, 2 \text{ or } 3 \quad \left(\text{Bound of } \mathbf{f} = (f_1, f_2) \text{ or } \mathbf{f} = (f_1, f_2, f_3)\right)
\end{cases}
\end{aligned}
\tag{26}
$$

where ρ and η are the density and dynamic viscosity of the fluid, respectively; $\mathbf{u}$ is the fluid velocity; p is the pressure; $-\alpha\mathbf{u}$ is the artificial Darcy force; $\mathbf{u}_D$ is the known velocity distribution on the boundary Γ_D; $\mathbf{g}$ is the known stress distribution on the boundary Γ_N; Ω is the design domain; ω_1 and ω_2 are the weights of the two integrations of A and B in the objective; θ_{Vol} is the upper bound of the volume fraction of the fluid; f_{li} and f_{hi}, chosen based on the engineering requirement, are the lower and upper bounds of the i-th component of the control variable $\mathbf{f}$, respectively; the control variable $\mathbf{f}$ is filtered by the Helmholtz filter; $\widetilde{\mathbf{f}}$ is the filtered control variable; the filtered design variable is projected by the threshold method (Eq. (17)) and $\widetilde{\overline{\gamma}}$ is the projected design variable. In Eq. (26), the control variable $\mathbf{f}$ corresponds to the variable u in Eq. (1); the velocity $\mathbf{u}$, the pressure p, the filtered variables $\widetilde{\gamma}$ and $\widetilde{\mathbf{f}}$ correspond to the components of the state variable y in Eq. (1).

In order to avoid the fluid flow driven by the body force in the approximated solid region, the physical control is penalized using the power-law approach, i.e. $\widetilde{\mathbf{f}}\,\widetilde{\overline{\gamma}}^{m}$, where m is the penalty chosen to be 3 [79]. The penalized filtered control variable $\widetilde{\mathbf{f}}\,\widetilde{\overline{\gamma}}^{m}$ is called physical control representing the body force loaded on the fluid. In the design domain, the interpolation of the impermeability α is [19]

$$
\alpha(\widetilde{\overline{\gamma}}) = \alpha_S\left[1 - \widetilde{\overline{\gamma}}(1+q)/(q+\widetilde{\overline{\gamma}})\right] \tag{27}
$$

where α_S, chosen as a high but finite number to approximate the solid and ensure the numerical stability, is the impermeability of the solid phase; q is a positive number used to tune the convexity of the interpolation. According to Eq. (5), the following substitution is performed for the control variable:

$$
f_i = f_{li} + f_{01_i}(f_{hi} - f_{li}), \quad f_{01_i} \in [0, 1],\ i = 1, 2 \text{ or } 3 \tag{28}
$$

where f_{01_i} is the i-th component of the projected control variable. When the iterative procedure is converged, the physical density $\widetilde{\overline{\gamma}}$ and filtered control $\widetilde{\mathbf{f}}$ can be obtained based on the obtained distributions of γ and $\mathbf{f}_{01}$, respectively.

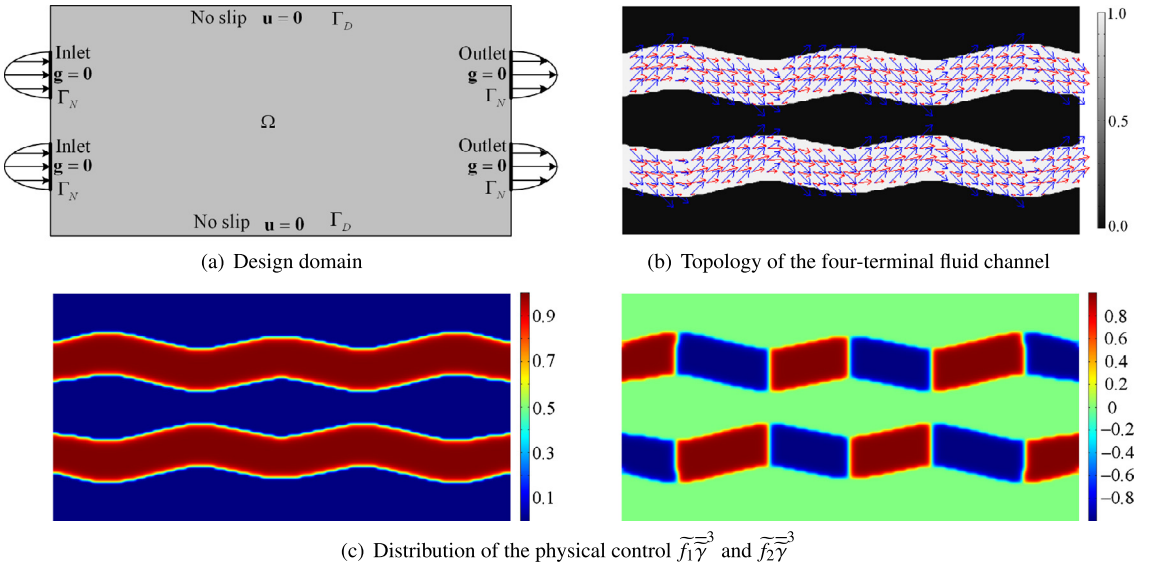

(a) Design domain (b) Topology of the four-terminal fluid channel

(c) Distribution of the physical control $\widetilde{f}_1\overline{\widetilde{\gamma}}^3$ and $\widetilde{f}_2\overline{\widetilde{\gamma}}^3$

Fig. 7. (a) Design domain of the fluid flow problem, where the size is 2×1; (b) topology of the four-terminal fluid channel in the optimal match, where the blue arrows and red arrows represent the physical control vectors and velocity vectors respectively; (c) distribution of the physical control in the optimal match. (For interpretation of the references to color in this figure, the reader is referred to the web version of this article.)

Based on the adjoint method in Section 2.2, the adjoint equations of the Navier–Stokes equations are obtained as:

$$\begin{aligned}
&\rho(\nabla\mathbf{u}\cdot\mathbf{u}_a)-\rho\mathbf{u}\cdot\nabla\mathbf{u}_a-\nabla\cdot\left[\eta\left(\nabla\mathbf{u}_a+\nabla\mathbf{u}_a^{\mathrm{T}}\right)\right]+\nabla p_a=-\omega_1\left(\frac{\partial A}{\partial\mathbf{u}}-\nabla\cdot\frac{\partial A}{\partial\nabla\mathbf{u}}\right)-\alpha\mathbf{u}_a,\quad \text{in } \Omega\\
&-\nabla\cdot\mathbf{u}_a=-\omega_1\frac{\partial A}{\partial p},\quad \text{in } \Omega\\
&\mathbf{u}_a=-\omega_2\frac{\partial B}{\partial p}\mathbf{n},\quad \text{on } \Gamma_D\\
&\left[p_a\mathbf{I}-\eta\left(\nabla\mathbf{u}_a+\nabla\mathbf{u}_a^{\mathrm{T}}\right)\right]\cdot\mathbf{n}=\omega_1\frac{\partial A}{\partial\nabla\mathbf{u}}\cdot\mathbf{n}+\omega_2\frac{\partial B}{\partial\mathbf{u}}+\rho(\mathbf{u}\cdot\mathbf{n})\mathbf{u}_a,\quad \text{on } \Gamma_N
\end{aligned}\tag{29}$$

where $\mathbf{u}_a$ and p_a are the adjoint variables of $\mathbf{u}$ and p, respectively. The adjoint equations of the Helmholtz filters for the design and control variables are obtained as:

$$\begin{aligned}
&-r^2\nabla\cdot\nabla\widetilde{\gamma}_a+\widetilde{\gamma}_a=-\left(\omega_1\frac{\partial A}{\partial\overline{\widetilde{\gamma}}}+\frac{\partial\alpha}{\partial\overline{\widetilde{\gamma}}}\mathbf{u}\cdot\mathbf{u}_a-m\overline{\widetilde{\gamma}}^{m-1}\widetilde{\mathbf{f}}\cdot\mathbf{u}_a\right)\frac{\partial\overline{\widetilde{\gamma}}}{\partial\widetilde{\gamma}},\quad \text{in } \Omega\\
&r^2\nabla\widetilde{\gamma}_a\cdot\mathbf{n}=-\omega_2\frac{\partial B}{\partial\overline{\widetilde{\gamma}}}\frac{\partial\overline{\widetilde{\gamma}}}{\partial\widetilde{\gamma}},\quad \text{on } \partial\Omega
\end{aligned}\tag{30}$$

$$\begin{aligned}
&-r^2\nabla\cdot\nabla\widetilde{\mathbf{f}}_a+\widetilde{\mathbf{f}}_a=-\omega_1\frac{\partial A}{\partial\widetilde{\mathbf{f}}}+\overline{\widetilde{\gamma}}^m\mathbf{u}_a,\quad \text{in } \Omega\\
&r^2\nabla\widetilde{\mathbf{f}}_a\cdot\mathbf{n}=-\omega_2\frac{\partial B}{\partial\widetilde{\mathbf{f}}},\quad \text{on } \partial\Omega
\end{aligned}\tag{31}$$

where $\widetilde{\gamma}_a$ and $\widetilde{\mathbf{f}}_a$ are the adjoint variables of $\widetilde{\gamma}$ and $\widetilde{\mathbf{f}}$, respectively. And the adjoint derivatives are obtained as:

$$\begin{aligned}
&\left.\frac{DJ}{D\gamma}\right|_{\Omega}=-\widetilde{\gamma}_a\\
&\left.\frac{DJ}{D\mathbf{f}_{01}}\right|_{\Omega}=-\widetilde{\mathbf{f}}_a\cdot\frac{\partial\mathbf{f}}{\partial\mathbf{f}_{01}}
\end{aligned}\tag{32}$$

In the following, one four-terminal fluid channel is optimized to demonstrate the combination of topology optimization and optimal distribution control method for the fluid flow problem. The design domain, discretized by 200×100 rectangular elements, is shown in Fig. 7(a). The objective is to maximize the kinetic energy of the fluid and the flux of the flow by setting $A = -1/2\rho\mathbf{u}^2$ in Ω and $B = \mathbf{u}\cdot\mathbf{n}$ on the inlet boundaries. The parameter choices are listed in Table 5. The optimal match is obtained with the fluid topology and distribution of the physical control variable shown in Figs. 7(b) and 7(c) respectively.

Table 5
Parameter setting for solving the variational problem of fluid flow in the four-terminal channel. s is the reference coordinate on the inlet boundary.

ρ	η	$\mathbf{u}_D$	$\mathbf{g}$	m	r	θ_{Vol}	α_S	q	ξ	ω_1	ω_2	f_{l1}	f_{h1}	f_{l2}	f_{h2}
1	1	$(4s(1-s), 0)$	$\mathbf{0}$	3	1×10^{-2}	0.4	1×10^4	1	0.5	0.9	0.1	-1	1	-1	1

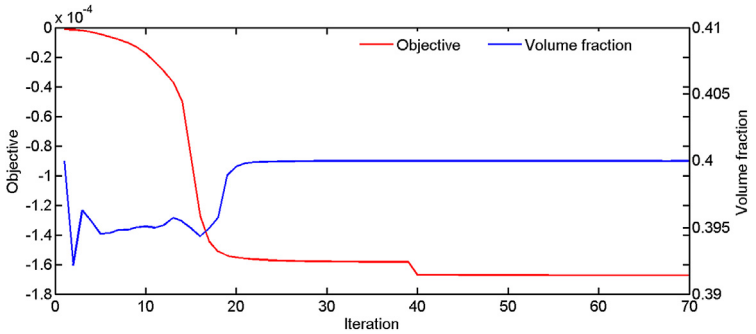

Fig. 8. Convergent histories of the objective values and volume constraint. The cost of CPU time is 1.55 h.

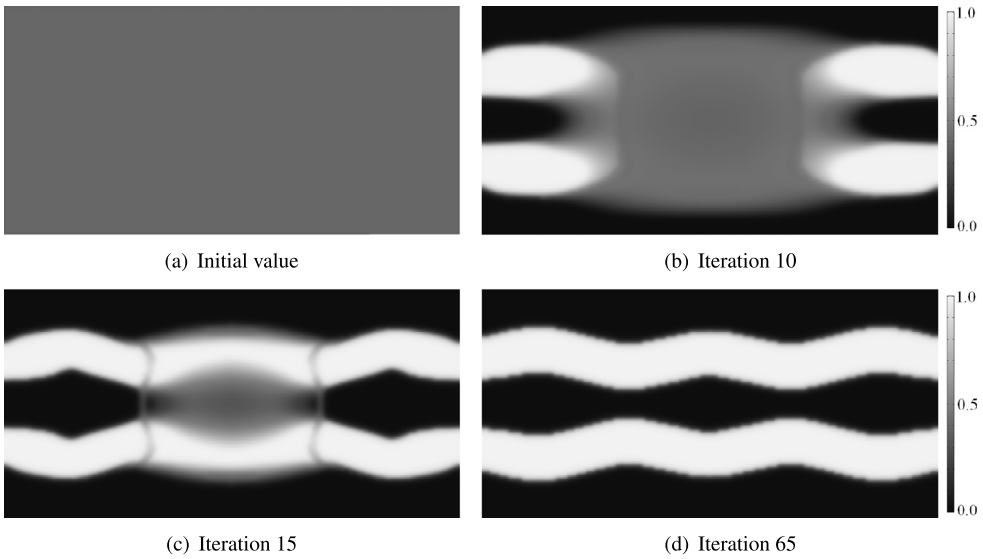

(a) Initial value (b) Iteration 10

(c) Iteration 15 (d) Iteration 65

Fig. 9. Snapshots for the evolution of the physical density.

The convergent histories of the objective values and volume fraction are plotted in Fig. 8. Snapshots for the evolution of the physical density and physical control are shown in Figs. 9, 10 and 11, respectively.

From the distribution of the physical control vectors representing the body force (blue arrows in Fig. 7(b)) and the velocity vectors (red arrows in Fig. 7(b)) in the fluid topology, one can see that the physical control tries to reach the maximum value of the bound constraint of the control and the fluid topology makes the direction of the velocity vectors trend to be consistent with the direction of the physical control to maximize the kinetic energy of the fluid and the flux at the inlet boundaries. On the physical realizability, the obtained physical control as a body force can be realized by imposing electromagnetic force on the ions in the liquid solution [34,80,81].

To check the optimality of the obtained match of the topology and control in Fig. 7, the similar method is adopted as that in Section 4.1.1. The optimal topology in Fig. 12(a) is obtained using the topology optimization method by fixing the physical control as shown in Fig. 7(c); the optimal control in Fig. 12(b) is obtained using the optimal distribution control method by fixing the physical density as shown in Fig. 7(b); and the objective values corresponding to Figs. 7(b), 12(a) and 12(c) are listed in Table 6. Based on the consistency of the values in Table 6, the optimality is confirmed for the obtained match between the topology and control.

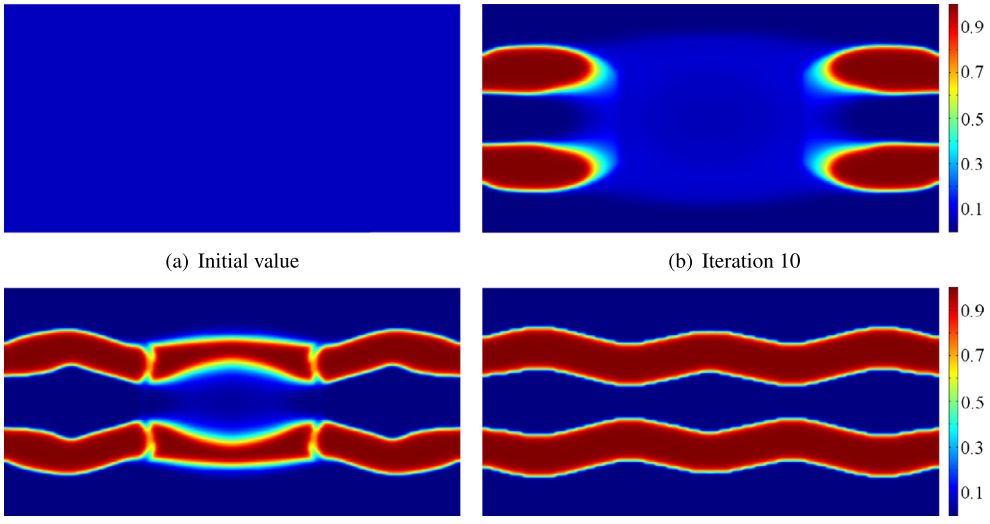

Fig. 10. Snapshots for the evolution of $\widetilde{f}_1\widetilde{\overline{\gamma}}^3$.

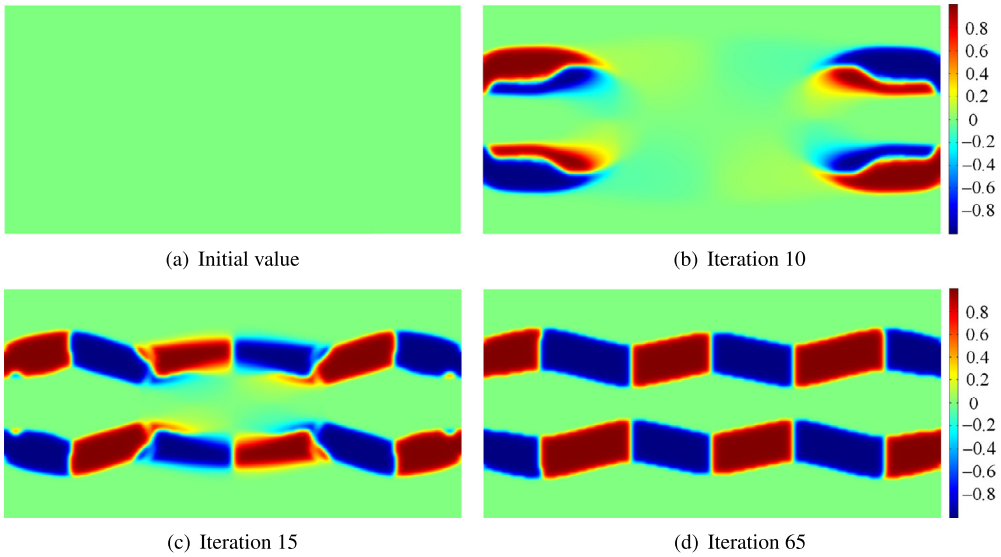

Fig. 11. Snapshots for the evolution of $\widetilde{f}_2\widetilde{\overline{\gamma}}^3$.

4.2. Combination of topology optimization and optimal boundary control

4.2.1. Fluid flow

In this section, the combination of topology optimization and optimal boundary control method is tested for the fluid flow problem. At present, the work of the topology optimization in the area of fluid flow was performed in a design domain with fixed boundary condition [19,51,68]. Meanwhile, the optimal boundary control of fluid flow was implemented in a fixed fluid domain [82–84]. Therefore, the problem, on how to find the reasonable match between the topology of the fluid domain and boundary control, is encountered. Then the following variational problem is constructed for the fluid flow to find the optimal match between the fluid topology and boundary control:

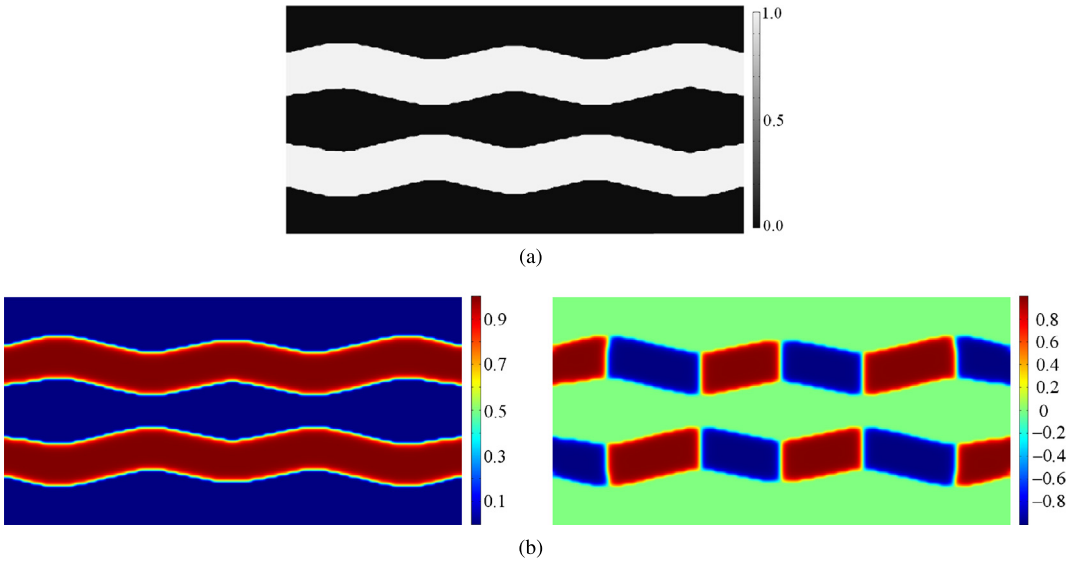

Fig. 12. (a) Optimal topology computed by fixing the physical distribution control as shown in Fig. 7(d); (b) optimal distribution of the physical control computed by fixing the topology as shown in Fig. 7(b).

Table 6
Objective values corresponding to Figs. 7(b), 12(a) and 12(b).

Fig. 7(b)	Fig. 12(a)	Fig. 12(b)
1.6802×10^{-4}	1.6815×10^{-4}	1.6745×10^{-4}

$$
\begin{aligned}
&\text{Find:} \quad (\gamma, \mathbf{u}_C)\\
&\text{Min:} \quad J(\mathbf{u}, p; \gamma, \mathbf{u}_C) = \int_{\Omega} \omega_1 A(\mathbf{u}, \nabla\mathbf{u}, p; \overline{\overline{\gamma}})\,\mathrm{d}\Omega + \int_{\Gamma_D \cup \Gamma_N} \omega_2 B(\mathbf{u}, p; \overline{\overline{\gamma}})\,\mathrm{d}\Gamma + \int_{\Gamma_C} \omega_3 C(p; \overline{\overline{\gamma}}, \mathbf{u}_C)\,\mathrm{d}\Gamma\\
&\text{S.t.} \quad \begin{cases}
\begin{cases}
\rho\mathbf{u}\cdot\nabla\mathbf{u} - \nabla\cdot\left[\eta\left(\nabla\mathbf{u} + \nabla\mathbf{u}^{\mathrm{T}}\right)\right] + \nabla p = -\alpha\mathbf{u}, & \text{in } \Omega\\
-\nabla\cdot\mathbf{u} = 0, & \text{in } \Omega\\
\mathbf{u} = \mathbf{u}_D, & \text{on } \Gamma_D\\
\mathbf{u} = \mathbf{u}_C, & \text{on } \Gamma_C\\
\left[p\mathbf{I} - \eta\left(\nabla\mathbf{u} + \nabla\mathbf{u}^{\mathrm{T}}\right)\right]\cdot\mathbf{n} = \mathbf{g}, & \text{on } \Gamma_N
\end{cases} \quad \text{(Navier–Stokes equations)}\\
\begin{cases}
-r^2\nabla\cdot\nabla\widetilde{\gamma} + \widetilde{\gamma} = \gamma, & \text{in } \Omega\\
\nabla\widetilde{\gamma}\cdot\mathbf{n} = 0, & \text{on } \partial\Omega
\end{cases} \quad \text{(Filter of } \gamma\text{)}\\
\int_{\Omega} \overline{\overline{\gamma}}\,\mathrm{d}\Omega \leqslant \theta_{Vol} V_0 \quad \text{(Volume constraint)}\\
0 \leqslant \gamma \leqslant 1 \quad \text{(Bound of } \gamma\text{)}\\
u_{Cli}(\mathbf{x}) \leqslant u_{Ci} \leqslant u_{Chi}(\mathbf{x}), \quad \mathbf{x} \in \Gamma_C \text{ and } i = 1, 2 \text{ or } 3 \quad \left(\text{Bound of } \mathbf{u}_C = (u_{C1}, u_{C2}) \text{ or } \mathbf{u}_C = (u_{C1}, u_{C2}, u_{C3})\right)
\end{cases}
\end{aligned}
\tag{33}
$$

where the topology optimization of the flow is also implemented by adding the artificial Darcy force to the Navier–Stokes equations; ω_1, ω_2 and ω_3 are the weights of the three integrations of A, B and C in the objective; $\mathbf{u}_C$ is the control variable on the boundary Γ_C; u_{Cli} and u_{Chi}, chosen based on the engineering requirement, are the lower and upper bounds of the i-th component of the control variable $\mathbf{u}_C$, respectively. In Eq. (33), the boundary control variable $\mathbf{u}_C$ corresponds to the variable u in Eq. (1); the velocity $\mathbf{u}$, the pressure p and filtered design variable $\widetilde{\gamma}$ correspond to the components of the state variable y in Eq. (1). The design variable γ is filtered by the Helmholtz filter. The filtered design variable is projected by the threshold method (Eq. (17)). The interpolation of the impermeability α is the same as that in Eq. (27). According to Eq. (5), the following projection is performed for the boundary control variable:

$$u_{Ci} = u_{Cli} + u_{C01_i}(u_{Chi} - u_{Cli}), \quad u_{C01_i} \in [0, 1],\ i = 1, 2 \text{ or } 3 \tag{34}$$

where u_{C01_i} is the i-th component of the projected boundary control variable.

Based on the adjoint method in Section 2.2, the adjoint equations of the Navier–Stokes equations are obtained as:

$$\begin{aligned}
&\rho(\nabla\mathbf{u}\cdot\mathbf{u}_a)-\rho\mathbf{u}\cdot\nabla\mathbf{u}_a-\nabla\cdot\left[\eta\left(\nabla\mathbf{u}_a+\nabla\mathbf{u}_a^{\mathrm{T}}\right)\right]+\nabla p_a=-\omega_1\left(\frac{\partial A}{\partial\mathbf{u}}-\nabla\cdot\frac{\partial A}{\partial\nabla\mathbf{u}}\right)-\alpha\mathbf{u}_a,\quad \text{in } \Omega\\
&-\nabla\cdot\mathbf{u}_a=-\omega_1\frac{\partial A}{\partial p},\quad \text{in } \Omega\\
&\mathbf{u}_a=-\omega_2\frac{\partial B}{\partial p}\mathbf{n},\quad \text{on } \Gamma_D\\
&\mathbf{u}_a=-\omega_3\frac{\partial C}{\partial p}\mathbf{n},\quad \text{on } \Gamma_C\\
&\left[p_a\mathbf{I}-\eta\left(\nabla\mathbf{u}_a+\nabla\mathbf{u}_a^{\mathrm{T}}\right)\right]\cdot\mathbf{n}=\omega_1\frac{\partial A}{\partial\nabla\mathbf{u}}\cdot\mathbf{n}+\omega_2\frac{\partial B}{\partial\mathbf{u}}+\rho(\mathbf{u}\cdot\mathbf{n})\mathbf{u}_a,\quad \text{on } \Gamma_N
\end{aligned}\tag{35}$$

The adjoint equation of the Helmholtz filter for the design variable is obtained as:

$$\begin{aligned}
&-r^2\nabla\cdot\nabla\widetilde{\gamma}_a+\widetilde{\gamma}_a=-\left(\omega_1\frac{\partial A}{\partial\overline{\overline{\widetilde{\gamma}}}}+\frac{\partial\alpha}{\partial\overline{\overline{\widetilde{\gamma}}}}\mathbf{u}\cdot\mathbf{u}_a\right)\frac{\partial\overline{\overline{\widetilde{\gamma}}}}{\partial\widetilde{\gamma}},\quad \text{in } \Omega\\
&r^2\nabla\widetilde{\gamma}_a\cdot\mathbf{n}=-\omega_2\frac{\partial B}{\partial\overline{\overline{\widetilde{\gamma}}}}\frac{\partial\overline{\overline{\widetilde{\gamma}}}}{\partial\widetilde{\gamma}},\quad \text{on } \Gamma_D\cup\Gamma_N\\
&r^2\nabla\widetilde{\gamma}_a\cdot\mathbf{n}=-\omega_3\frac{\partial C}{\partial\overline{\overline{\widetilde{\gamma}}}}\frac{\partial\overline{\overline{\widetilde{\gamma}}}}{\partial\widetilde{\gamma}},\quad \text{on } \Gamma_C
\end{aligned}\tag{36}$$

And the adjoint derivatives are obtained as:

$$\begin{aligned}
&\left.\frac{DJ}{D\gamma}\right|_{\Omega}=-\widetilde{\gamma}_a\\
&\left.\frac{DJ}{D\mathbf{u}_{C01}}\right|_{\Gamma_C}=\left[\omega_3\frac{\partial C}{\partial\mathbf{u}_C}+\eta\left(\nabla\mathbf{u}_a+\nabla\mathbf{u}_a^{\mathrm{T}}\right)\cdot\mathbf{n}-p_a\mathbf{n}\right]\cdot\frac{\partial\mathbf{u}_C}{\partial\mathbf{u}_{C01}}
\end{aligned}\tag{37}$$

To demonstrate the combination of topology optimization and optimal boundary control method for the fluid flow problem, the backstep flow with Reynolds number 100 is optimized. In the optimal boundary control of the backstep flow, the objective is usually chosen to damp out the vorticity development near the corner [34]. At the same time, the dissipation of the backstep flow is usually considered to ensure the smoothness of the fluid channel in topology optimization. Therefore, the objective of the variational problem in Eq. (33) is set to be $A=[\eta/2(\nabla\mathbf{u}+\nabla\mathbf{u}^{\mathrm{T}}):(\nabla\mathbf{u}+\nabla\mathbf{u}^{\mathrm{T}})+\alpha\mathbf{u}^2]+(\nabla\times\mathbf{u})^2/2$, $B=0$ and $C=\mathbf{u}_C^2/2$ to find the optimal match between the fluid topology of the corner region and the boundary control. The design domain is set as shown in Fig. 13(a), discretized by 8100 rectangular elements. The parameter choices are listed in Table 7. By solving the variational problem, the fluid topology (Fig. 13(b)) and the matched boundary control are obtained (Fig. 13(c)). The convergent histories of the objective values and volume constraint are shown in Fig. 14. Snapshots for the evolution of the physical density and boundary control are shown in Figs. 15 and 16, respectively. From the streamline distribution in Fig. 17(b), one can conclude that the optimal match between the fluid topology and boundary control has damped out the vorticity development near the corner of the backstep flow effectively.

The optimality is checked for the obtained match between the fluid topology and boundary control. When the boundary control on Γ_C is fixed (Fig. 13(c)), the topology optimization is performed and the topology is obtained as shown in Fig. 18(a); when the topology is fixed (Fig. 13(b)), the optimal boundary control method is implemented and the boundary control is derived as shown in Fig. 18(b). The objective values corresponding to the results in Figs. 13, 18(a) and 18(b) are listed in Table 8. Based on the results in Fig. 13 and Fig. 18 and the consistency of the objective values in Table 8, the optimality is confirmed for the obtained match between the fluid topology and boundary control. When the topology optimization and optimal boundary control methods are utilized for the backstep flow separately, the optimal topology and optimal boundary control as well as the streamline distribution are obtained as shown in Figs. 19 and 20.

4.2.2. Compliance minimization

Compliance minimization has been the most mature area in topology optimization [7,13–17]. In most of the published papers, the compliance minimization is performed under the specified load, i.e. the optimal design is found to fit the given load. In this section, the combination of topology optimization and optimal boundary control method is used to find the optimal match between the material topology of compliant structure and distribution of the surface force loaded on the boundary. The corresponding variational problem is constructed as:

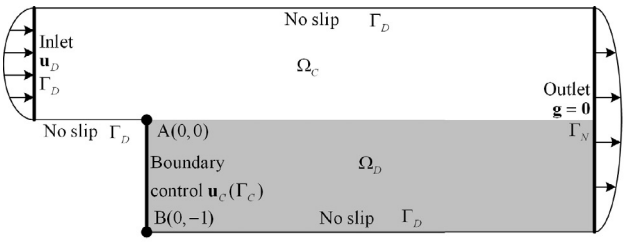

(a) Design domain

(b) Topology of the corner region

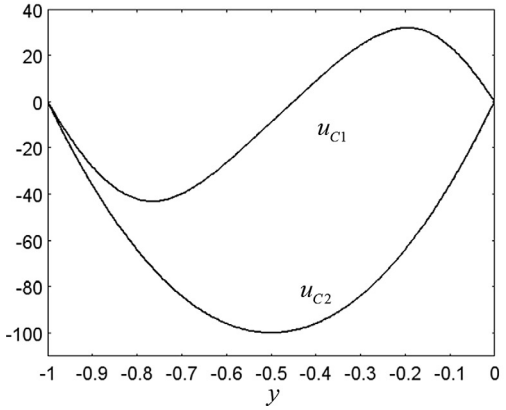

(c) Boundary control $\mathbf{u}_C = (u_{C1}, u_{C2})$

Fig. 13. (a) Design domain of the backstep flow, where Ω_D defined with the design variable γ is the design domain and $\Omega = \Omega_C \cup \Omega_D$ is the computational domain; (b) fluid topology of the corner region in the optimal match; (c) boundary control of the optimal match.

Table 7
Parameter setting for the optimization of the backstep flow. s is the reference coordinate on the corresponding boundary.

ρ	η	$\mathbf{u}_D$	$\mathbf{g}$	r	θ_{Vol}	α_S	q	ξ	ω_1	ω_2	ω_3
1	1	$(400s(1-s), 0)$	$\mathbf{0}$	1×10^{-2}	0.8	1×10^{4}	1	0.5	0.4	0	0.2

u_{Cl1}	u_{Ch1}	u_{Cl2}	u_{Ch2}
$-400s(1-s)$	$400s(1-s)$	$-400s(1-s)$	$400s(1-s)$

Find: $(\gamma, \boldsymbol{\sigma}_C)$

Min: $$J(\mathbf{v};\gamma,\boldsymbol{\sigma}_C)=\int_{\Omega}\omega_1 A(\mathbf{v},\nabla\mathbf{v};\overline{\widetilde{\gamma}})\,\mathrm{d}\Omega+\int_{\Gamma_D\cup\Gamma_N}\omega_2 B(\mathbf{v};\overline{\widetilde{\gamma}})\,\mathrm{d}\Gamma+\int_{\Gamma_C}\omega_3 C(\mathbf{v};\overline{\widetilde{\gamma}},\boldsymbol{\sigma}_C)\,\mathrm{d}\Gamma$$

S.t.
$$\begin{cases}
\begin{cases}\nabla\cdot\left[-\mathbf{K}\left(\nabla\mathbf{v}+\nabla\mathbf{v}^{\mathrm{T}}\right)\right]=\mathbf{0}, & \text{in } \Omega\\ \mathbf{v}=\mathbf{v}_D, & \text{on } \Gamma_D\\ \mathbf{K}\left(\nabla\mathbf{v}+\nabla\mathbf{v}^{\mathrm{T}}\right)\cdot\mathbf{n}=\boldsymbol{\sigma}_C, & \text{on } \Gamma_C\\ \mathbf{K}\left(\nabla\mathbf{v}+\nabla\mathbf{v}^{\mathrm{T}}\right)\cdot\mathbf{n}=\boldsymbol{\sigma}, & \text{on } \Gamma_N\end{cases} & \text{(Elastics)}\\
\begin{cases}-r^2\nabla\cdot\nabla\widetilde{\gamma}+\widetilde{\gamma}=\gamma, & \text{in } \Omega\\ \nabla\widetilde{\gamma}\cdot\mathbf{n}=0, & \text{on } \partial\Omega\end{cases} & \text{(Filter of } \gamma)\\
\int_{\Omega}\overline{\widetilde{\gamma}}\,\mathrm{d}\Omega\leqslant\theta_{Vol}V_0 & \text{(Volume constraint)}\\
0\leqslant\gamma\leqslant1 & \text{(Bound of } \gamma)\\
\sigma_{Cli}(\mathbf{x})\leqslant\sigma_{Ci}\leqslant\sigma_{Chi}(\mathbf{x}), \quad \mathbf{x}\in\Gamma_C,\ i=1,2 \text{ or } 3 & \left(\text{Bound of } \boldsymbol{\sigma}_C=(\sigma_{C1},\sigma_{C2}) \text{ or } \boldsymbol{\sigma}_C=(\sigma_{C1},\sigma_{C2},\sigma_{C3})\right)
\end{cases} \tag{38}$$

where the topology optimization of the compliance is implemented using the SIMP method [7,16]; $\mathbf{K}$ is the stiffness tensor of the isotropic linear elastic material; $\mathbf{v}$ is the displacement; $\mathbf{v}_D$ is the known displacement on Γ_D; $\boldsymbol{\sigma}_C$, representing stress distribution, is the control variable on the boundary Γ_C; $\boldsymbol{\sigma}$ is the known stress distribution on the boundary Γ_N;

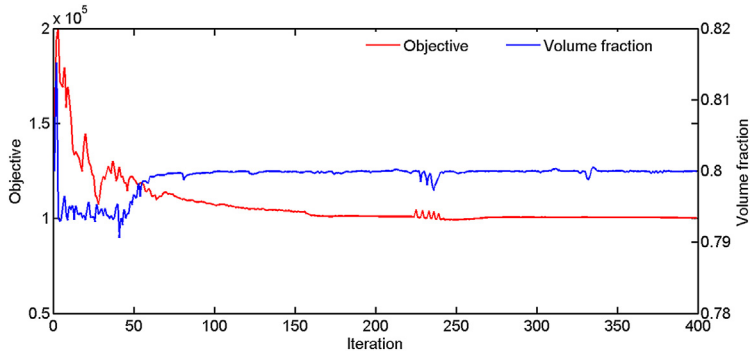

Fig. 14. Convergent histories of the objective values and volume constraint. The objective value corresponding to the optimality is 1.0016×10^5. The cost of CPU time is 5.08 h.

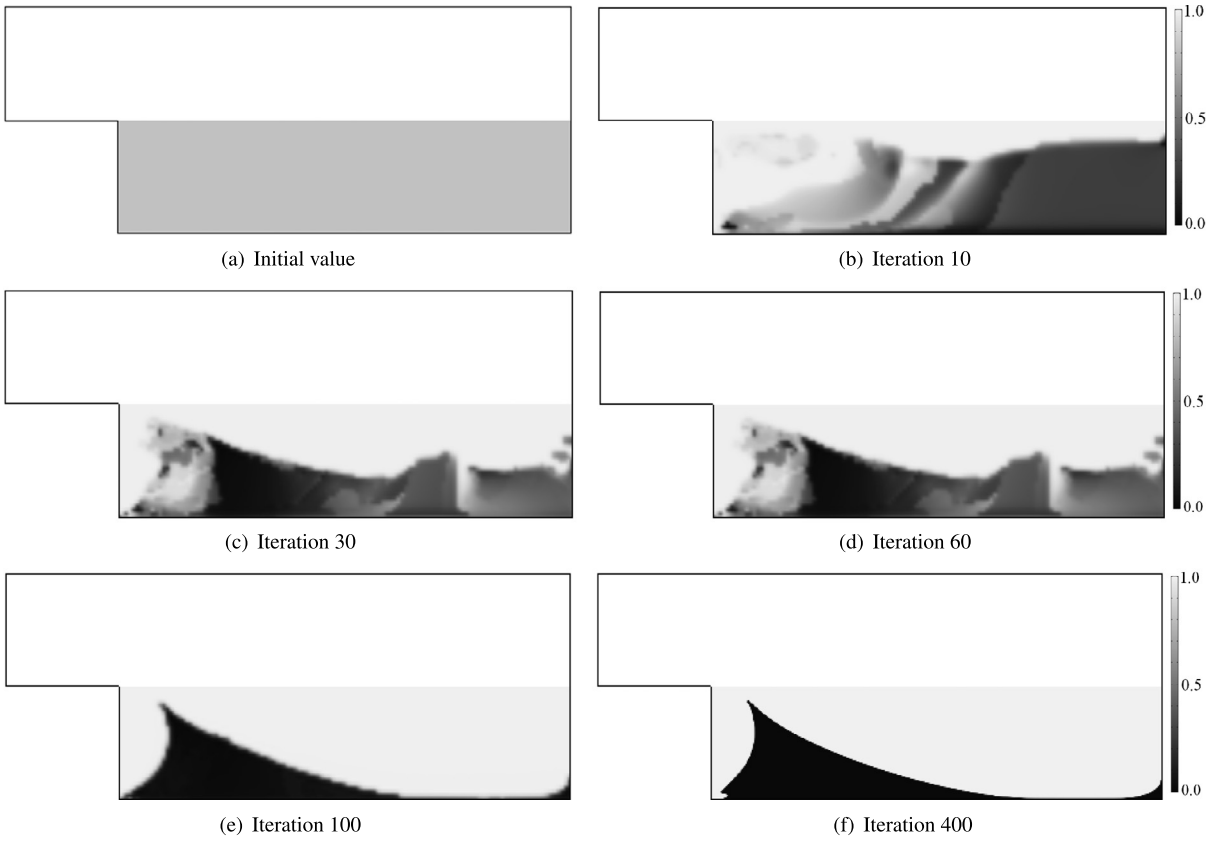

Fig. 15. Snapshots for the evolution of the physical density.

σ_{Cli} and σ_{Chi}, chosen based on the engineering requirement, are the lower and upper bounds of the i-th component of the boundary control variable $\boldsymbol{\sigma}_C$, respectively. In Eq. (38), the boundary control variable $\boldsymbol{\sigma}_C$ corresponds to the control variable u in Eq. (1); the displacement $\mathbf{v}$ and filtered design variable $\widetilde{\gamma}$ correspond to the components of the state variable y in Eq. (1). The design variable γ is filtered and projected with the same method as that in the former sections. The interpolation of Young's module E in the stiffness tensor $\mathbf{K}$ is:

$$E = E_0 \widetilde{\overline{\gamma}}^m \tag{39}$$

where E_0 is the Young's module of the material; m is the penalty chosen to be 3 [16]. For the boundary control variable, the following projection is performed according to Eq. (5):

$$\sigma_{Ci} = \sigma_{Cli} + \sigma_{C01i}(\sigma_{Chi} - \sigma_{Cli}), \quad \sigma_{C01i} \in [0,1], \ i = 1, 2 \text{ or } 3 \tag{40}$$

where σ_{C01i} is the i-th component of the projected boundary control variable.

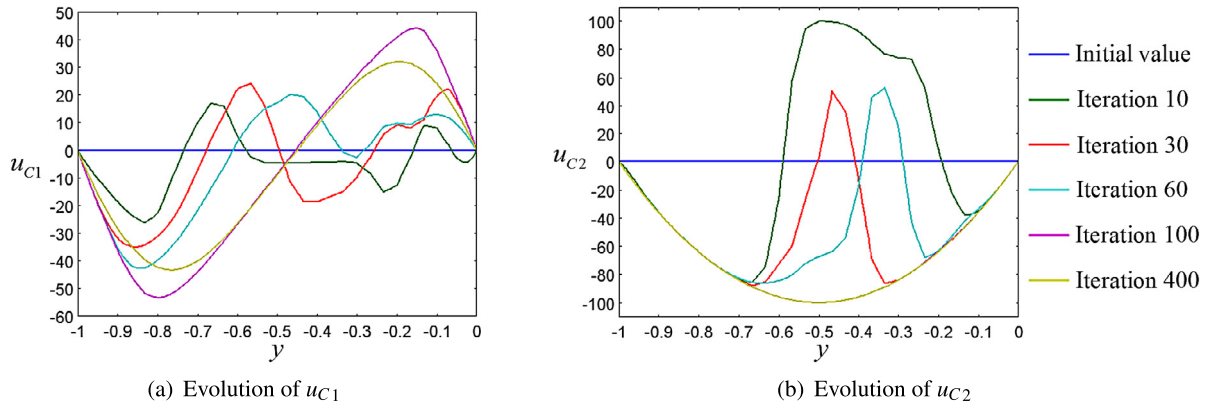

(a) Evolution of u_{C1} (b) Evolution of u_{C2}

Fig. 16. Snapshots for the evolution of $\mathbf{u}_C$ on Γ_C.

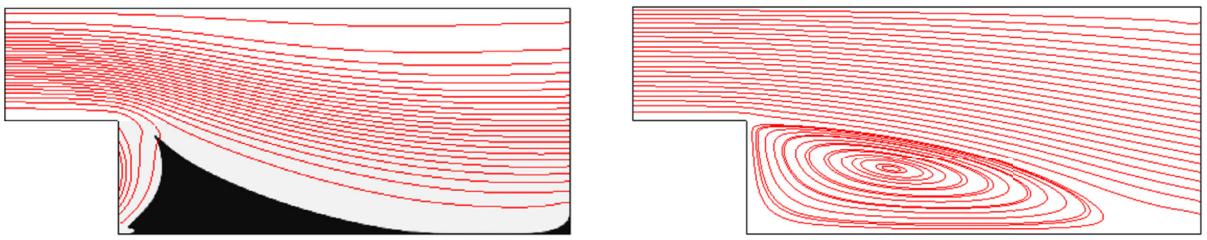

(a) (b)

Fig. 17. (a) Streamline distribution in the backstep flow optimized by combining the topology optimization and optimal boundary control method; (b) streamline distribution in the backstep flow without optimization.

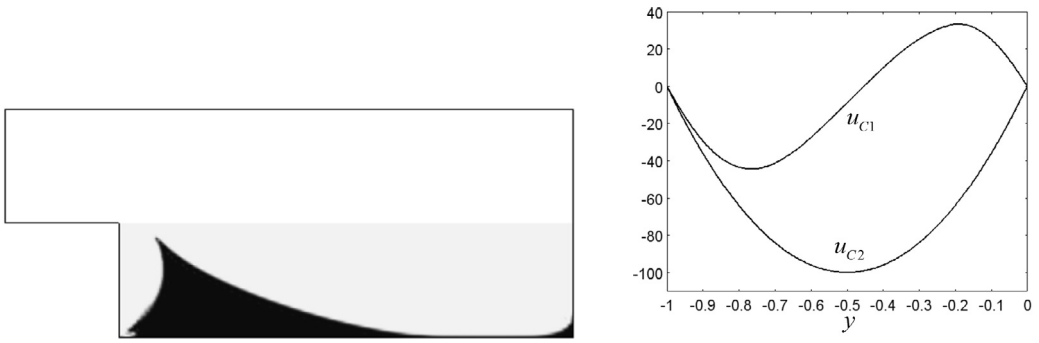

(a) (b)

Fig. 18. (a) Optimal topology of the backstep flow obtained by the topology optimization method, where the boundary control on Γ_C is fixed as shown in Fig. 13(c); (b) optimal boundary control obtained by the optimal boundary control method, where the topology of the backstep flow is fixed as shown in Fig. 13(b).

Based on the adjoint method in Section 2.2, the adjoint equation of the elastics equation is obtained as:

$$\begin{aligned}
&\nabla\cdot\left[-\mathbf{K}\left(\nabla\mathbf{v}_a+\nabla\mathbf{v}_a^{\mathrm{T}}\right)\right]=-\omega_1\left(\frac{\partial A}{\partial\mathbf{v}}-\nabla\cdot\frac{\partial A}{\partial\nabla\mathbf{v}}\right),\quad \text{in } \Omega\\
&\mathbf{v}_a=\mathbf{0},\quad \text{on } \Gamma_D\\
&\mathbf{K}\left(\nabla\mathbf{v}_a+\nabla\mathbf{v}_a^{\mathrm{T}}\right)\cdot\mathbf{n}=-\left(\omega_1\frac{\partial A}{\partial\nabla\mathbf{v}}\cdot\mathbf{n}+\omega_2\frac{\partial B}{\partial\mathbf{v}}\right),\quad \text{on } \Gamma_N\\
&\mathbf{K}\left(\nabla\mathbf{v}_a+\nabla\mathbf{v}_a^{\mathrm{T}}\right)\cdot\mathbf{n}=-\left(\omega_1\frac{\partial A}{\partial\nabla\mathbf{v}}\cdot\mathbf{n}+\omega_3\frac{\partial C}{\partial\mathbf{v}}\right),\quad \text{on } \Gamma_C
\end{aligned}\tag{41}$$

where $\mathbf{v}_a$ is the adjoint variable of the displacement $\mathbf{v}$. The adjoint equation of the Helmholtz filter for the design variable is:

Table 8
Objective values corresponding to Figs. 13(b), 18(a) and 18(b).

Fig. 13(b)	Fig. 18(a)	Fig. 18(b)
1.0008×10^5	1.0011×10^5	1.0009×10^5

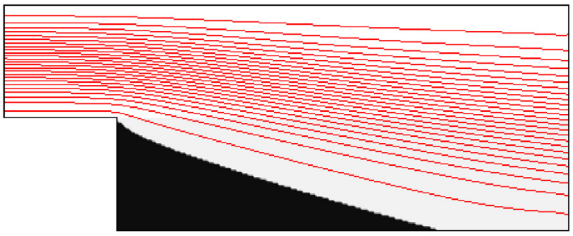

Fig. 19. Topology and streamline distribution of the backstep flow obtained by the topology optimization method.

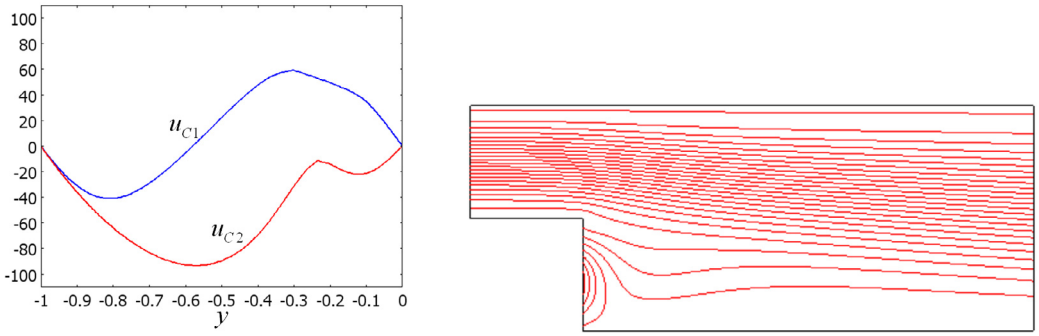

Fig. 20. (a) Optimal control of the backstep flow obtained by the optimal boundary control method; (b) streamline distribution of the backstep flow with the optimal control.

$$
\begin{aligned}
&-r^2\nabla\cdot\nabla\widetilde{\gamma}_a+\widetilde{\gamma}_a=-\left[\omega_1\frac{\partial A}{\partial\overline{\overline{\gamma}}}+\frac{\partial\mathbf{K}}{\partial\overline{\overline{\gamma}}}\left(\nabla\mathbf{v}+\nabla\mathbf{v}^{\mathrm{T}}\right):\nabla\mathbf{v}_a\right]\frac{\partial\overline{\overline{\gamma}}}{\partial\widetilde{\gamma}},\quad \text{in } \Omega\\
&r^2\nabla\widetilde{\gamma}_a\cdot\mathbf{n}=-\omega_2\frac{\partial B}{\partial\overline{\overline{\gamma}}}\frac{\partial\overline{\overline{\gamma}}}{\partial\widetilde{\gamma}},\quad \text{on } \Gamma_D\cup\Gamma_N\\
&r^2\nabla\widetilde{\gamma}_a\cdot\mathbf{n}=-\omega_3\frac{\partial C}{\partial\overline{\overline{\gamma}}}\frac{\partial\overline{\overline{\gamma}}}{\partial\widetilde{\gamma}},\quad \text{on } \Gamma_C
\end{aligned}
\tag{42}
$$

And the adjoint derivatives are:

$$
\begin{aligned}
&\left.\frac{DJ}{D\gamma}\right|_{\Omega}=-\widetilde{\gamma}_a\\
&\left.\frac{DJ}{D\boldsymbol{\sigma}_{C01}}\right|_{\Gamma_C}=\left(\omega_3\frac{\partial C}{\partial\boldsymbol{\sigma}_C}-\mathbf{v}_a\right)\cdot\frac{\partial\boldsymbol{\sigma}_C}{\partial\boldsymbol{\sigma}_{C01}}
\end{aligned}
\tag{43}
$$

To demonstrate the combination of topology optimization and optimal boundary control method for compliant mechanism design, a cantilever is optimized to find the optimal match between the material topology and distribution of the surface force. The design domain of the cantilever is shown in Fig. 21(a) discretized by 80×40 rectangular elements, and the parameter choices are listed in Table 9. The objective is chosen to minimize the strain energy in the cantilever, by setting $A = 1/2\mathbf{K}(\nabla\mathbf{v}+\nabla\mathbf{v}^{\mathrm{T}}):(\nabla\mathbf{v}+\nabla\mathbf{v}^{\mathrm{T}})$, $B=0$ and $C=0$. After solving the variational problem, the optimal match of the material topology and distribution of the surface force are obtained as shown in Figs. 21(b) and 21(c). The convergent histories of the objective values and volume constraint are shown in Fig. 22. Snapshots for the evolution of the physical density is shown in Fig. 23.

The schematic of the controlled surface force in Fig. 21(b) and the bending moments of σ_{C1} and σ_{C2} in Fig. 21(d) demonstrate that the bending moment of σ_{C1} counteracts that of σ_{C2} and the bending moment of σ_{C2} exceeds that of σ_{C1}. Therefore, σ_{C2} takes the value of the lower limit σ_{l2} and σ_{C1} takes the upper and lower limits to try its best to balance the bending moment of σ_{C2} and decrease the strain energy of the deformed cantilever. As the bound of σ_{C1} is

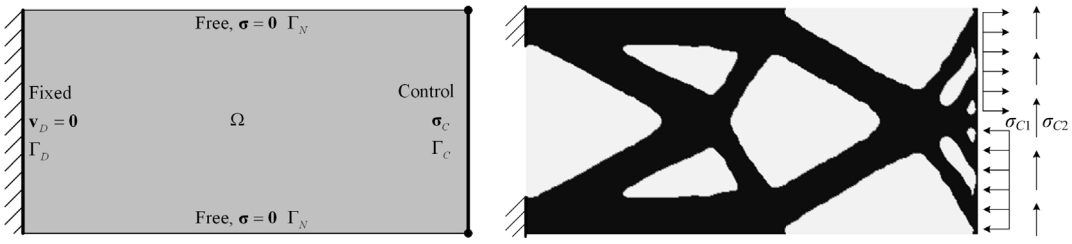

(a) Design domain (b) Material topology

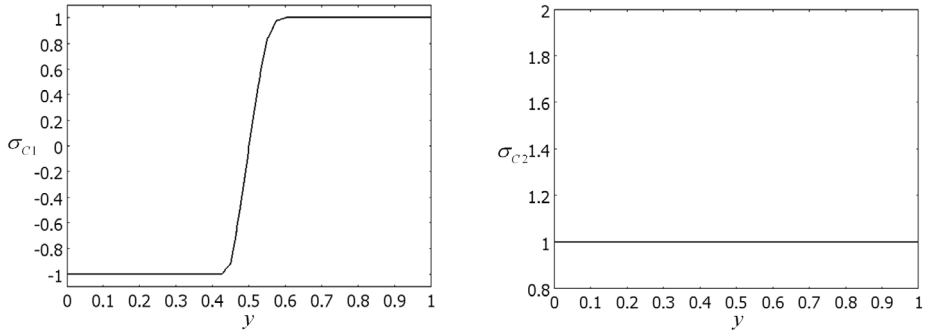

(c) Distribution of the surface force $\boldsymbol{\sigma}_C = (\sigma_{C1}, \sigma_{C2})$

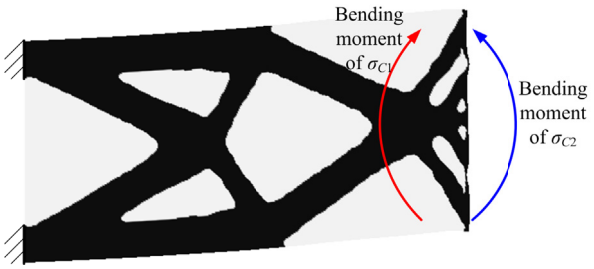

(d) Bending moment of the obtained distribution of the surface force

Fig. 21. (a) Design domain of the cantilever, where the size is 2×1; (b) material topology of the cantilever; (c) distribution of the surface force $\boldsymbol{\sigma}_C = (\sigma_{C1}, \sigma_{C2})$; (d) bending moments of σ_{C1} and σ_{C2}. The objective value corresponding to the optimality is 1.2685×10^{-10}. The cost of CPU time is 0.2141 h.

Table 9
Parameter setting for solving the variational problem corresponding to the compliance minimization of the cantilever.

$\mathbf{v}_D$	$\boldsymbol{\sigma}$	E_0	ν	m	r	θ_{Vol}	ξ	ω_1	ω_2	ω_3	σ_{l1}	σ_{h1}	σ_{l2}	σ_{h2}
$\mathbf{0}$	$\mathbf{0}$	2.0×10^{11}	0.33	3	1×10^{-2}	0.5	0.5	1	0	0	-1	1	1	2

relaxed to be $\sigma_{l1} = -8$ and $\sigma_{h1} = 8$, the material topology and the matched distribution of the surface force are shown in Fig. 24. Fig. 24(b) shows that the upper and lower limits of σ_{C1} are not reached, i.e. the bound of σ_{C1} is inactive. Then the counteraction of σ_{C1} to σ_{C2} reaches the maximum. This can be confirmed from the objective value 7.3620×10^{-11}, which is 41.96% lower than 1.2685×10^{-10} corresponding to the bound active case in Fig. 21. This example shows that the inactivity of the bound of the control variable can be ensured by respectively choosing reasonable high and low values for the upper and lower limits in the bound constraint.

4.3. Test for transient problem

Transient problems are ubiquitous in engineering. This section is focused on the combination of topology optimization and optimal control method for the transient problem. The topology optimization and optimal control method have been developed for the transient problem, respectively. For the transient problems, the topology optimization is performed in the interpolated design domain with fixed distribution and boundary inputs; and optimal control is implemented in the fixed domain defined with physical field. To find the optimal match of the material topology and control variable for the transient problem, the topology optimization and optimal control method are combined and tested for the unsteady fluid flow problem in this paper. Topology optimization method for the unsteady flow has been developed in [52,85], recently.

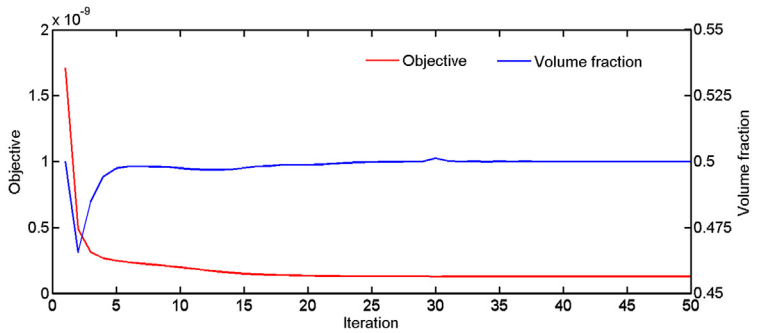

Fig. 22. Convergent histories of the objective values and volume constraint.

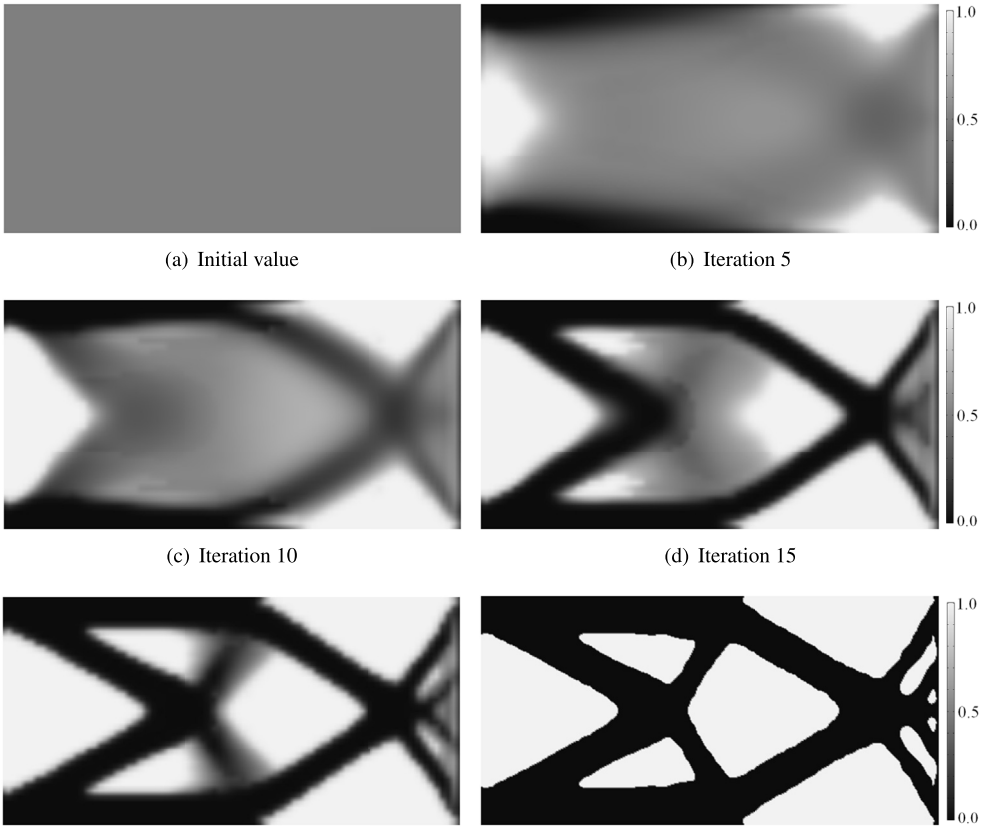

(a) Initial value (b) Iteration 5

(c) Iteration 10 (d) Iteration 15

(e) Iteration 20 (f) Iteration 50

Fig. 23. Snapshots for the evolution of the material topology.

Then based on the topology optimization and optimal control method for the unsteady flow, the following variational problem is constructed to find the optimal match:

$$\text{Find:} \quad (\gamma, \mathbf{f}, \mathbf{u}_C)$$

$$\text{Min:} \quad J(\mathbf{u}, p; \gamma, \mathbf{f}, \mathbf{u}_C) = \int_0^{\Theta} \int_{\Omega} \omega_1 A(\mathbf{u}, \nabla \mathbf{u}, p; \overline{\overline{\gamma}}, \widetilde{\mathbf{f}}) \, \mathrm{d}\Omega \, \mathrm{d}t + \int_0^{\Theta} \int_{\Gamma_D \cup \Gamma_N} \omega_2 B(\mathbf{u}, p; \overline{\overline{\gamma}}, \widetilde{\mathbf{f}}) \, \mathrm{d}\Gamma \, \mathrm{d}t + \int_0^{\Theta} \int_{\Gamma_C} \omega_3 C(p; \overline{\overline{\gamma}}, \widetilde{\mathbf{f}}, \mathbf{u}_C) \, \mathrm{d}\Gamma \, \mathrm{d}t$$

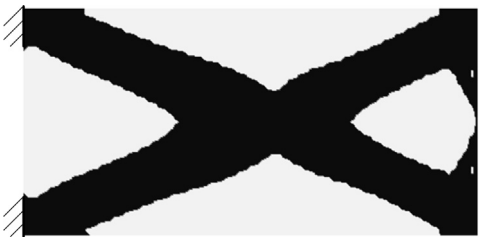

(a) Material topology

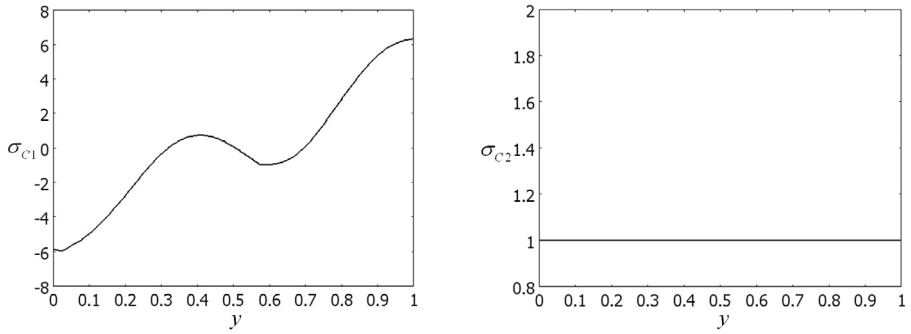

(b) Distribution of the surface force $\boldsymbol{\sigma}_C = (\sigma_{C1}, \sigma_{C2})$

Fig. 24. (a) Material topology of the cantilever; (b) distribution of the surface force $\boldsymbol{\sigma}_C = (\sigma_{C1}, \sigma_{C2})$. The objective value corresponding to the optimality is 7.3620×10^{-11}. The cost of CPU time is 0.6109 h.

$$
\text{S.t.}\quad
\begin{cases}
\begin{cases}
\rho \frac{\partial \mathbf{u}}{\partial t} + \rho \mathbf{u} \cdot \nabla \mathbf{u} - \nabla \cdot \left[\eta\left(\nabla \mathbf{u} + \nabla \mathbf{u}^{\mathrm{T}}\right)\right] + \nabla p = -\alpha \mathbf{u} + \widetilde{\mathbf{f}}\widetilde{\overline{\gamma}}^{m}, & \text{in } \Omega \\
-\nabla \cdot \mathbf{u} = 0, & \text{in } \Omega \\
\mathbf{u}|_{t=0} = \mathbf{u}_0, & \text{in } \Omega \\
\mathbf{u} = \mathbf{u}_D, & \text{on } \Gamma_D \\
\mathbf{u} = \mathbf{u}_C, & \text{on } \Gamma_C \\
\left[p\mathbf{I} - \eta\left(\nabla \mathbf{u} + \nabla \mathbf{u}^{\mathrm{T}}\right)\right] \cdot \mathbf{n} = \mathbf{g}, & \text{on } \Gamma_N
\end{cases} \quad \text{(Navier–Stokes equations)} \\
\begin{cases} -r^2 \nabla \cdot \nabla \widetilde{\gamma} + \widetilde{\gamma} = \gamma, & \text{in } \Omega \\ \nabla \widetilde{\gamma} \cdot \mathbf{n} = 0, & \text{on } \partial\Omega \end{cases} \quad \text{(Filter of } \gamma\text{)} \\
\begin{cases} -r^2 \nabla \cdot \nabla \widetilde{\mathbf{f}} + \widetilde{\mathbf{f}} = \mathbf{f}, & \text{in } \Omega \\ \nabla \widetilde{\mathbf{f}} \cdot \mathbf{n} = \mathbf{0}, & \text{on } \partial\Omega \end{cases} \quad \text{(Filter of } \mathbf{f}\text{)} \\
\int_\Omega \overline{\widetilde{\gamma}}\, \mathrm{d}\Omega \leqslant \theta_{Vol} V_0 \quad \text{(Volume constraint)} \\
0 \leqslant \gamma \leqslant 1 \quad \text{(Bound of } \gamma\text{)} \\
f_{li}(\mathbf{x}) \leqslant f_i \leqslant f_{hi}(\mathbf{x}), \quad \mathbf{x} \in \Omega,\ i = 1, 2 \text{ or } 3 \quad \left(\text{Bound of } \mathbf{f} = (f_1, f_2) \text{ or } \mathbf{f} = (f_1, f_2, f_3)\right) \\
u_{Cli}(\mathbf{x}) \leqslant u_{Ci} \leqslant u_{Chi}(\mathbf{x}), \quad \mathbf{x} \in \Gamma_C,\ i = 1, 2 \text{ or } 3 \quad \left(\text{Bound of} \mathbf{u}_C = (u_{C1}, u_{C2}) \text{ or } \mathbf{u}_C = (u_{C1}, u_{C2}, u_{C3})\right)
\end{cases}
\tag{44}
$$

where t is the time; $[0, \Theta]$ is the considered time interval; $\mathbf{u}_0$ is the initial distribution of the fluid velocity. When solving the unsteady incompressible Navier–Stokes equations, the design variable γ is time independent because the layout of the fluid domain is kept unchanged; and $\mathbf{f}$ and $\mathbf{u}_C$ are time dependent, because different velocity distributions at different time needs different distributions of the controls. The design variable γ and the control variable $\mathbf{f}$ are filtered by Helmholtz filters. The projection of the filtered design variable $\widetilde{\gamma}$ is performed by the threshold method as in Eq. (17). The physical distribution control is penalized by $\widetilde{\overline{\gamma}}^m$, where the penalty m is chosen to be 3. And the bound constraints of the distribution control $\mathbf{f}$ and boundary control $\mathbf{u}_c$ are projected using Eqs. (28) and (34), respectively.

Based on the adjoint method in Section 2.2, the adjoint equations of the Navier–Stokes equations are obtained as:

$$
\begin{aligned}
&-\rho \frac{\partial \mathbf{u}_a}{\partial t} + \rho(\nabla \mathbf{u} \cdot \mathbf{u}_a) - \rho \mathbf{u} \cdot \nabla \mathbf{u}_a - \nabla \cdot \left[\eta\left(\nabla \mathbf{u}_a + \nabla \mathbf{u}_a^{\mathrm{T}}\right)\right] + \nabla p_a = -\omega_1 \left(\frac{\partial A}{\partial \mathbf{u}} - \nabla \cdot \frac{\partial A}{\partial \nabla \mathbf{u}}\right) - \alpha \mathbf{u}_a, \quad \text{in } \Omega \\
&-\nabla \cdot \mathbf{u}_a = -\omega_1 \frac{\partial A}{\partial p}, \quad \text{in } \Omega \\
&\mathbf{u}_a|_{t=\Theta} = \mathbf{0}, \quad \text{in } \Omega
\end{aligned}
$$

Table 10
Parameter setting for solving the variational problem of the unsteady flow rectifier. s is the reference coordinate on the corresponding boundary; $U(t)$ and $h(t)$ are functions of the time t as shown in Fig. 25.

ρ	η	$\mathbf{u}_D$	$\mathbf{g}$	Θ	m	r	θ_{Vol}	α_S	q	ξ	ω_1	ω_2	ω_3
1	1	$(4s(1-s)U(t),0)$	$\mathbf{0}$	1	3	1×10^{-2}	0.4	1×10^{4}	1	0.5	1×10^{-5}	$1-2\omega_1$	ω_1

f_{l1}	f_{h1}	f_{l2}	f_{h2}	u_{Cl1}	u_{Ch1}	u_{Cl2}	u_{Ch2}
-1	1	-1	1	$-4s(1-s)h(t)$	$4s(1-s)h(t)$	$-4s(1-s)h(t)$	$4s(1-s)h(t)$

$$\mathbf{u}_a=-\omega_2\frac{\partial B}{\partial p}\mathbf{n},\quad \text{on } \Gamma_D$$
$$\mathbf{u}_a=-\omega_3\frac{\partial C}{\partial p}\mathbf{n},\quad \text{on } \Gamma_C$$
$$\left[p_a\mathbf{I}-\eta\left(\nabla\mathbf{u}_a+\nabla\mathbf{u}_a^{\mathrm{T}}\right)\right]\cdot\mathbf{n}=\omega_1\frac{\partial A}{\partial\nabla\mathbf{u}}\cdot\mathbf{n}+\omega_2\frac{\partial B}{\partial\mathbf{u}}+\rho(\mathbf{u}\cdot\mathbf{n})\mathbf{u}_a,\quad \text{on } \Gamma_N \tag{45}$$

The transient adjoint Eqs. (45) are terminal value problems, where the value of $\mathbf{u}_a$ at the terminal time Θ is specified and the transient solver is implemented from the time Θ to 0. The adjoint equations of the Helmholtz filters can be obtained as:

$$-r^2\nabla\cdot\nabla\widetilde{\gamma}_a+\widetilde{\gamma}_a=-\frac{1}{\Theta}\int_0^{\Theta}\left(\omega_1\frac{\partial A}{\partial\overline{\widetilde{\gamma}}}+\frac{\partial\alpha}{\partial\overline{\widetilde{\gamma}}}\mathbf{u}\cdot\mathbf{u}_a-m\overline{\widetilde{\gamma}}^{m-1}\widetilde{\mathbf{f}}\cdot\mathbf{u}_a\right)\frac{\partial\overline{\widetilde{\gamma}}}{\partial\widetilde{\gamma}}\,\mathrm{d}t,\quad \text{in } \Omega$$
$$r^2\nabla\widetilde{\gamma}_a\cdot\mathbf{n}=-\frac{1}{\Theta}\int_0^{\Theta}\omega_2\frac{\partial B}{\partial\overline{\widetilde{\gamma}}}\frac{\partial\overline{\widetilde{\gamma}}}{\partial\widetilde{\gamma}}\,\mathrm{d}t,\quad \text{on } \Gamma_D\cup\Gamma_N$$
$$r^2\nabla\widetilde{\gamma}_a\cdot\mathbf{n}=-\frac{1}{\Theta}\int_0^{\Theta}\omega_3\frac{\partial C}{\partial\overline{\widetilde{\gamma}}}\frac{\partial\overline{\widetilde{\gamma}}}{\partial\widetilde{\gamma}}\,\mathrm{d}t,\quad \text{on } \Gamma_C \tag{46}$$
$$-r^2\nabla\cdot\nabla\widetilde{\mathbf{f}}_a+\widetilde{\mathbf{f}}_a=-\omega_1\frac{\partial A}{\partial\widetilde{\mathbf{f}}}+\overline{\widetilde{\gamma}}^m\mathbf{u}_a,\quad \text{in } \Omega$$
$$r^2\nabla\widetilde{\mathbf{f}}_a\cdot\mathbf{n}=-\omega_2\frac{\partial B}{\partial\widetilde{\mathbf{f}}},\quad \text{on } \Gamma_D\cup\Gamma_N$$
$$r^2\nabla\widetilde{\mathbf{f}}_a\cdot\mathbf{n}=-\omega_3\frac{\partial C}{\partial\widetilde{\mathbf{f}}},\quad \text{on } \Gamma_C \tag{47}$$

From Eqs. (46) and (47), one can see that the adjoint variable $\widetilde{\gamma}_a$ is time independent and $\widetilde{\mathbf{f}}_a$ is time dependent. The adjoint derivatives of the objective functional in Eq. (44) are:

$$\left.\frac{DJ}{D\gamma}\right|_{\Omega}=-\Theta\widetilde{\gamma}_a$$
$$\left.\frac{DJ}{D\mathbf{f}_{01}}\right|_{\Omega}=-\widetilde{\mathbf{f}}_a\cdot\frac{\partial\mathbf{f}}{\partial\mathbf{f}_{01}}$$
$$\left.\frac{DJ}{D\mathbf{u}_{C01}}\right|_{\Gamma_C}=\left[\omega_3\frac{\partial C}{\partial\mathbf{u}_C}+\eta\left(\nabla\mathbf{u}_a+\nabla\mathbf{u}_a^{\mathrm{T}}\right)\cdot\mathbf{n}-p_a\mathbf{n}\right]\cdot\frac{\partial\mathbf{u}_C}{\partial\mathbf{u}_{C01}} \tag{48}$$

In the following, a flow rectifier is optimized to demonstrate the combination of topology optimization and optimal control method for the transient problem. The design domain is shown in Fig. 26(a) discretized by 100×100 rectangular elements. The parameter choices are listed in Table 10. The integrated functionals in the objective are set to be $A=1/2\eta(\nabla\mathbf{u}+\nabla\mathbf{u}^{\mathrm{T}}):(\nabla\mathbf{u}+\nabla\mathbf{u}^{\mathrm{T}})+\alpha\mathbf{u}^2+(\widetilde{\mathbf{f}}\overline{\widetilde{\gamma}})^2$ in Ω, $B=(\mathbf{u}\cdot\mathbf{n}-u_{rn})^2$ on Γ_N and $C=\mathbf{u}_C^2$ on Γ_C, where u_{rn} is the desired velocity distribution in the outward normal direction of the outlet Γ_N. This setting of the multi-objective is to rectify the outward normal velocity distribution on Γ_N approaching the desired distribution u_{rn} and minimize the dissipation power of the flow and the scope of the physical control $\mathbf{f}$ and $\mathbf{u}_C$, simultaneously. u_{rn} is set as $4s(1-s)V(t)$, where s is the reference coordinate on Γ_N and $V(t)$ represents the time dependent relation shown in Fig. 25. The known velocity imposed on the inlet is $\mathbf{u}_D=(4s(1-s)U(t),0)$, where $U(t)$ represents the time dependent relation shown in Fig. 25.

By solving the variational problem in the time interval $[0,1]$, the optimal match of the fluid topology (Fig. 26(b)), physical distribution control (Figs. 27 and 28) and boundary control (Fig. 29) are obtained. From the obtained fluid topology

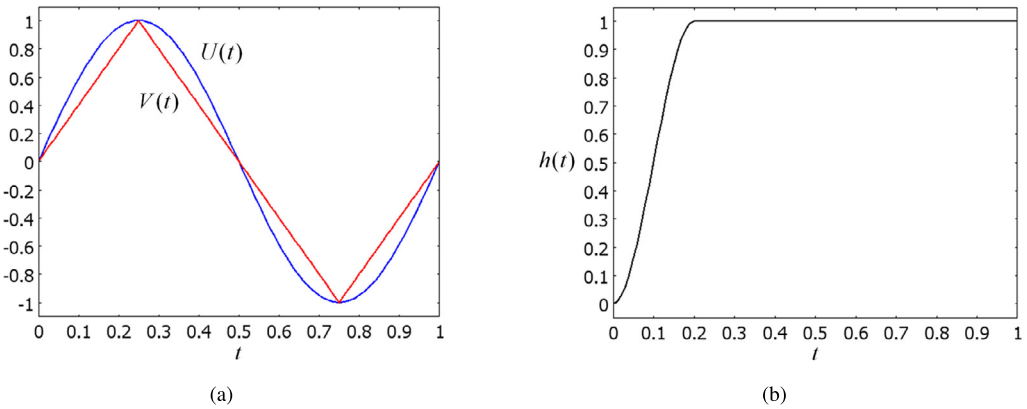

(a) (b)

Fig. 25. Plotting of the functions $U(t)$, $V(t)$ and $h(t)$.

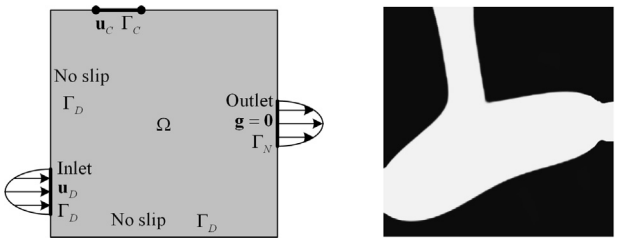

(a) Design domain (b) Topology of the flow rectifier

Fig. 26. (a) Design domain of the flow rectifier; (b) topology of the flow rectifier in the optimal match. The objective value corresponding to the optimality is 2.9663×10^{-4}. The CPU time cost is 49.9901 h.

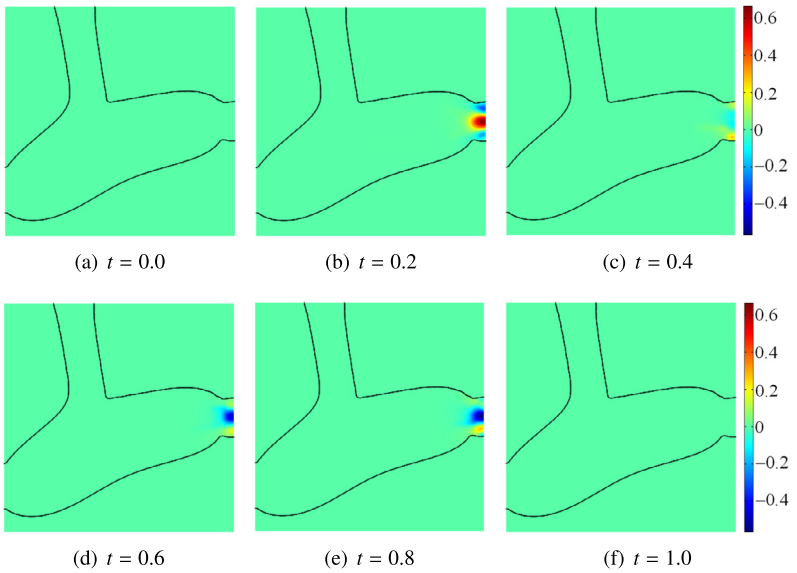

(a) $t = 0.0$ (b) $t = 0.2$ (c) $t = 0.4$

(d) $t = 0.6$ (e) $t = 0.8$ (f) $t = 1.0$

Fig. 27. Physical distribution control $\widetilde{f}_1 \widetilde{\gamma}^m$ at different time.

(Fig. 26(b)) and boundary control (Fig. 29), one can see that a ramose channel connected to the boundary Γ_C is produced to compensate the difference of the flux at the inlet Γ_D and outlet Γ_N and enforce the flux rate at the outlet Γ_N to be consistent with that of the desired velocity distribution. From the physical distribution control in Figs. 27 and 28, one can see that the physical distribution control mainly distributes near the outlet Γ_N to enforce the outward normal velocity distribution to be consistent with the desired case.

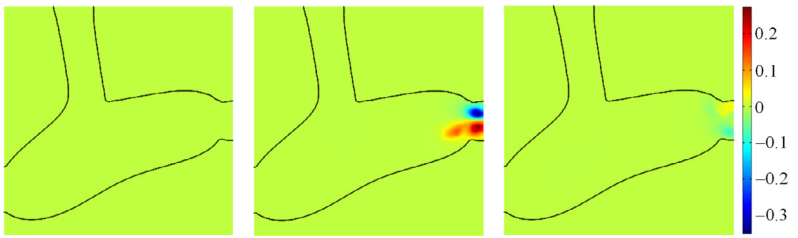

(a) $t = 0.0$ (b) $t = 0.2$ (c) $t = 0.4$

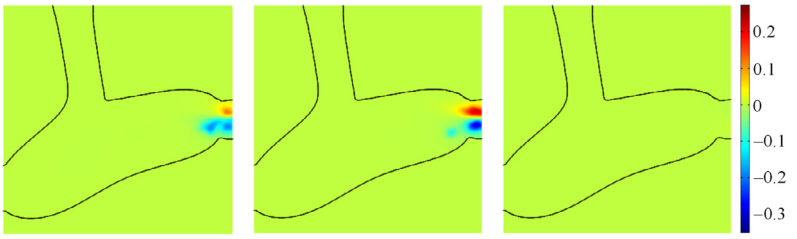

(d) $t = 0.6$ (e) $t = 0.8$ (f) $t = 1.0$

Fig. 28. Physical distribution control $\widetilde{f}_2\overline{\widetilde{\gamma}}^m$ at different time.

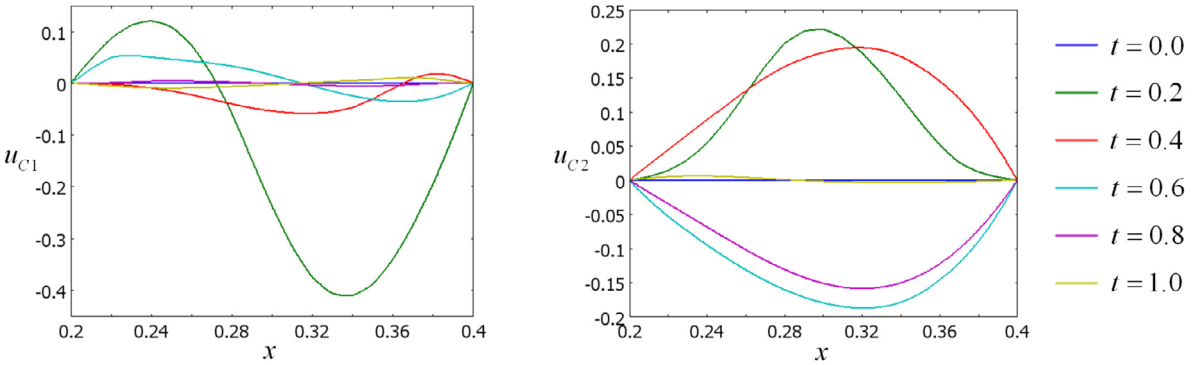

(a) u_{C1} (b) u_{C2}

Fig. 29. Boundary control $\mathbf{u}_C$ at different time.

5. Conclusion

The combination of topology optimization and optimal control method has been presented in this paper. By the presented combination, the optimal match between the material topology and control has been achieved. In this combination, the control variable is constrained by a bound constraint and the bound constraint is projected onto $[0, 1]$, which is the same as the bound constraint for the design variable in topology optimization, and this is convenient to use the method of moving asymptotes to evolve the design and control variables simultaneously. The corresponding variational problems are analyzed and solved using the adjoint method and iterative approach, respectively. In the numerical examples, the combination of topology optimization and optimal distribution control has been tested for the heat transfer and steady flow problems; the combination of topology optimization and optimal boundary control has been demonstrated by the steady flow and compliance minimization problems; and the combination method for the transient problem has been also discussed and demonstrated by the unsteady flow problem. Based on the combination of topology optimization and optimal control method, the freedom of the engineering design is enlarged, and the designer can give more reasonable design to cater for the engineering requirement.

Acknowledgements

The authors are grateful to Professor K. Svanberg for supply of the MMA codes. This work is supported by the National High Technology Research and Development Program (863 Program) of China (No. 2012AA040503), the National Natural Science Foundation of China (Nos. 50975272, 11034007, 51205381). This work is also supported by the SKLAO Open Fund in CIOMP. And the authors are also grateful to the reviewers' kind attention and valuable suggestions.

References

[1] O. Pironneau, On optimum profiles in Stokes flow, J. Fluid Mech. 59 (1973) 117–128.
[2] O. Pironneau, On optimum design in fluid mechanics, J. Fluid Mech. 64 (1974) 97–110.
[3] H.O. Fattorini, Time-optimal control of solutions of operational differential equation, SIAM J. Control 2 (1964) 54–59.
[4] A. Friedman, Optimal control of parabolic equations, J. Math. Anal. Appl. 18 (1967) 479–491.
[5] A.G. Butkovskii, Theory of Optimal Control of Distributed Parameter Systems, Elsevier, 1969.
[6] G.I.N. Rozvany, Aims, scope, methods, history and unified terminology of computer-aided topology optimization in structural mechanics, Struct. Multidiscip. Optim. 21 (2001) 90–108.
[7] M.P. Bendsoe, N. Kikuchi, Generating optimal topologies in optimal design using a homogenization method, Comput. Methods Appl. Mech. Eng. 71 (1988) 197–224.
[8] M.P. Bendsoe, O. Sigmund, Material interpolations in topology optimization, Arch. Appl. Mech. 69 (1999) 635–654.
[9] M.Y. Wang, X. Wang, D. Guo, A level set method for structural optimization, Comput. Methods Appl. Mech. Eng. 192 (2003) 227–246.
[10] G. Allaire, F. Jouve, A. Toader, Structural optimization using sensitivity analysis and a level-set method, J. Comput. Phys. 194 (2004) 363–393.
[11] Z. Liu, J.G. Korvink, Adaptive moving mesh level set method for structure optimization, Eng. Optim. 40 (2008) 529–558.
[12] X. Xing, P. Wei, M.Y. Wang, A finite element-based level set method for structural optimization, Int. J. Numer. Methods Eng. 82 (2010) 805–842.
[13] G.I.N. Rozvany, Shape and Layout Optimization of Structural Systems and Optimality Criteria Methods, Springer, 1994.
[14] G.I.N. Rozvany, Topology Optimization in Structural Mechanics, Springer, 1997.
[15] O. Sigmund, On the design of compliant mechanisms using topology optimization, Mech. Struct. Mach. 25 (1997) 495–526.
[16] O. Sigmund, A 99-line topology optimization code written in Matlab, Struct. Multidiscip. Optim. 21 (2000) 120–127.
[17] A. Saxena, Topology design of large displacement compliant mechanisms with multiple materials and multiple output ports, Struct. Multidiscip. Optim. 30 (2005) 477–490.
[18] M. Bendsøe, O. Sigmund, Topology Optimization-Theory, Methods and Applications, Springer, Berlin, 2003.
[19] T. Borrvall, J. Petersson, Topology optimization of fluid in Stokes flow, Int. J. Numer. Methods Fluids 41 (2003) 77–107.
[20] T. Nomura, K. Sato, K. Taguchi, T. Kashiwa, S. Nishiwaki, Structural topology optimization for the design of broadband dielectric resonator antennas using the finite difference time domain technique, Int. J. Numer. Methods Eng. 71 (2007) 1261–1296.
[21] O. Sigmund, K.G. Hougaard, Geometric properties of optimal photonic crystals, Phys. Rev. Lett. 100 (2008) 153904.
[22] M.B. Duhring, J.S. Jensen, O. Sigmund, Acoustic design by topology optimization, J. Sound Vib. 317 (2008) 557–575.
[23] W. Akl, A. El-Sabbagh, K. Al-Mitani, A. Baz, Topology optimization of a plate coupled with acoustic cavity, Int. J. Solids Struct. 46 (2008) 2060–2074.
[24] Q. Li, G.P. Steven, Y.M. Xie, O.M. Querin, Evolutionary topology optimization for temperature reduction of heat conducting fields, Int. J. Heat Mass Transf. 47 (23) (2004) 5071–5083.
[25] A. Gersborg-Hansen, M.P. Bendsoe, O. Sigmund, Topology optimization of heat conduction problems using the finite volume method, Struct. Multidiscip. Optim. 31 (2006) 251–259.
[26] S. Osher, J.A. Sethian, Front propagating with curvature dependent speed: Algorithms based on Hamilton–Jacobi formulations, J. Comput. Phys. 78 (1988) 12–49.
[27] S. Zhou, Q. Li, A variational level set method for the topology optimization of steady-state Navier–Stokes flow, J. Comput. Phys. 227 (2008) 10178–10195.
[28] X. Duan, Y. Ma, R. Zhang, Shape-topology optimization for Navier–Stokes problem using variational level set method, J. Comput. Appl. Math. 222 (2008) 487–499.
[29] J. Sokolowski, A. Zochowski, On the topological derivative in shape optimization, SIAM J. Control Optim. 37 (1999) 1241–1272.
[30] J. Sokolowski, A. Zochowski, Topological derivatives for elliptic problems, Inverse Probl. 15 (1999) 123–134.
[31] A.A. Novotny, R.A. Feijoo, E. Taroco, C. Padra, Topological sensitivity analysis, Comput. Methods Appl. Mech. Eng. 192 (2003) 803–829.
[32] M. Burger, B. Hackl, W. Ring, Incorporating topological derivatives into level set methods, J. Comput. Phys. 194 (2004) 344–362.
[33] S. Amstutz, Topological sensitivity analysis for some nonlinear PDE systems, J. Math. Pures Appl. 85 (2006) 540–557.
[34] S.S. Sritharan, Optimal Control of Viscous Flow, SIAM, Philadelphia, 1998.
[35] J.L. Lions, Optimal Control of Systems Governed by Partial Differential Equations, Spring-Verlag, New York, 1971.
[36] J.L. Lions, Some Aspects of the Optimal Control of Distributed Parameter Systems, SIAM, Philadelphia, 1972.
[37] J.L. Lions, Some Methods in the Mathematical Analysis of Systems and Their Control, Gordon & Breach, New York, 1981.
[38] N.U. Ahmed, K.L. Teo, Optimal Control of Distributed Parameter Systems, North–Holland, New York, 1981.
[39] V. Barbu, G. Da Prato, Hamilton Jacobi Equations in Hilbert Spaces, Pitman, Boston, 1983.
[40] A.V. Fursikov, On some control problems and results related to the unique solution of mixed problems by the three-dimensional Navier–Stokes and Euler equations, Dokl. Akad. Nauk SSSR 252 (1980) 1066–1070.
[41] A.V. Fursikov, Control problems and results on the unique solution of mixed problems by the three-dimensional Navier–Stokes and Euler equations, Math. Sb. 115 (1981) 281–306.
[42] A.V. Fursikov, Properties of solutions of certain extremum problems related to the Navier–Stokes and Euler equations, Math. Sb. 117 (1981) 323–349.
[43] A. Jameson, Computational aerodynamics for aircraft design, Math. Sb. 245 (1989) 361–371.
[44] R. Glowinski, A.J. Kearsley, T.W. Pan, J. Periaux, Numerical simulation and optimal shape for viscous flow by a fictitious domain method, Int. J. Numer. Methods Fluids 20 (1995) 695–711.
[45] K. Svanberg, The method of moving asymptotes: a new method for structural optimization, Int. J. Numer. Methods Eng. 24 (1987) 359–373.
[46] E. Zeidler, Nonlinear Functional Analysis and Its Applications. I, Fixed-Point Theorems, Springer, Berlin, 1986.
[47] M. Hinze, R. Pinnau, M. Ulbrich, S. Ulbrich, Optimization with PDE Constraints, Springer, Berlin, 2009.
[48] M.B. Giles, N.A. Pierce, An introduction to the adjoint approach to design, Flow Turbul. Combust. 65 (2000) 393–415.
[49] B. Mohammadi, O. Pironneau, Applied Shape Optimization for Fluids, Oxford University Press, 2010.
[50] http://www.comsol.com.
[51] L.H. Olesen, F. Okkels, H. Bruus, A high-level programming-language implementation of topology optimization applied to steady-state Navier–Stokes flow, Int. J. Numer. Methods Eng. 65 (2006) 975–1001.
[52] Y. Deng, Z. Liu, P. Zhang, Y. Liu, Y. Wu, Topology optimization of unsteady incompressible Navier–Stokes flow, J. Comput. Phys. 230 (2011) 6688–6708.
[53] B. Lazarov, O. Sigmund, Filters in topology optimization based on Helmholtz type differential equations, Int. J. Numer. Methods Eng. 86 (6) (2011) 765–781, http://dx.doi.org/10.1002/nme.3072.
[54] F. Wang, B.S. Lazarov, O. Sigmund, On projection methods, convergence and robust formulations in topology optimization, Struct. Multidiscip. Optim. 43 (2011) 767–784.
[55] S. Xu, Y. Cai, G. Cheng, Volume preserving nonlinear density filter based on heaviside functions, Struct. Multidiscip. Optim. 41 (2010) 495–505.
[56] J. Guest, J. Prevost, T. Belytschko, Achieving minimum length scale in topology optimization using nodal design variables and projection functions, Int. J. Numer. Methods Eng. 61 (2004) 238–254.

[57] O. Sigmund, Morphology-based black and white filters for topology optimization, Struct. Multidiscip. Optim. 33 (2007) 401–424.
[58] A. Kawamoto, T. Matsumori, S. Yamasaki, T. Nomura, T. Kondoh, S. Nishiwaki, Heaviside projection based topology optimization by a PDE-filtered scalar function, Struct. Multidiscip. Optim. 44 (1) (2011) 19–24, http://dx.doi.org/10.1007/s00158-010-0562-2.
[59] H.C. Elman, D.J. Silvester, A.J. Wathen, Finite Elements and Fast Iterative Solvers: With Applications in Incompressible Fluid Dynamics, Oxford University Press, 2006.
[60] Q. Li, G.P. Steven, O.M. Querin, Y.M. Xie, Shape and topology design for heat conduction by evolutionary structural optimization, Int. J. Heat Mass Transf. 42 (1999) 3361–3371.
[61] C. Zhuang, Z. Xiong, H. Ding, A level set method for topology optimization of heat conduction problem under multiple load cases, Comput. Methods Appl. Mech. Eng. 196 (2007) 1074–1084.
[62] F. Troltzsch, An SQP method for the optimal control of a nonlinear heat equation, Control Cybern. 23 (1994) 268–288.
[63] R.L. Panton, Incompressible Flow, Wiley, 1984.
[64] N. Aage, T.H. Poulsen, A. Gersborg-Hansen, O. Sigmund, Topology optimization of large scale stokes flow problems, Struct. Multidiscip. Optim. 35 (2008) 175–180.
[65] P.H. Guillaume, K.S. Idris, Topological sensitivity and shape optimization for the Stokes equations, SIAM J. Control Optim. 43 (2004) 1–31.
[66] J.K. Guest, J.H. Proevost, Topology optimization of creeping fluid flows using a Darcy–Stokes finite element, Int. J. Numer. Methods Eng. 66 (2006) 461–484.
[67] N. Wiker, A. Klarbring, T. Borrvall, Topology optimization of regions of Darcy and Stokes flow, Int. J. Numer. Methods Eng. 69 (2007) 1374–1404.
[68] A. Gersborg-Hansen, O. Sigmund, R.B. Haber, Topology optimization of channel flow problems, Struct. Multidiscip. Optim. 29 (2005) 1–12.
[69] A. Evgrafov, Topology optimization of slightly compressible fluids, Z. Angew. Math. Mech. 86 (2006) 46–62.
[70] G. Pingen, K. Maute, Optimal design for non-Newtonian flows using a topology optimization approach, Comput. Math. Appl. 59 (2010) 2340–2350.
[71] F. Okkels, H. Bruus, Scaling behavior of optimally structured catalytic microfluidic reactors, Phys. Rev. E 75 (2007) 1–4.
[72] C.S. Andreasen, A.R. Gersborg, O. Sigmund, Topology optimization of microfluidic mixers, Int. J. Numer. Methods Fluids 61 (2008) 498–513.
[73] Y. Deng, Z. Liu, P. Zhang, Y. Wu, J.G. Korvink, Optimization of no-moving part fluidic resistance microvalves with low Reynolds number, in: Proceedings IEEE International Conference on Micro Electro Mechanical Systems (MEMS), 2010, pp. 67–70.
[74] Y. Deng, Y. Wu, M. Xuan, J.G. Korvink, Z. Liu, Dynamic optimization of valveless micropump, in: Proceedings IEEE International Conference on Solid-State Sensors, Actuators, and Microsystems (Transducers), 2011, pp. 442–445.
[75] Z. Liu, Y. Deng, S. Lin, M. Xuan, Optimization of micro Venturi diode in steady flow at low Reynolds number, Eng. Optim. 44 (11) (2012) 1389–1404, http://dx.doi.org/10.1080/0305215X.2011.652100.
[76] Y. Deng, Z. Liu, P. Zhang, Y. Liu, Q. Gao, Y. Wu, A flexible layout design method for passive micromixers, Biomed. Microdevices 14 (5) (2012) 929–945, http://dx.doi.org/10.1007/s10544-012-9672-5.
[77] M. Sandro, Optimal boundary and distribution controls for the velocity tracking problem for Navier–Stokes flows, PhD thesis, May 1997, Blacksburg, Virginia.
[78] T. Slawig, PDE-constrained control using FEMLAB – Control of the Navier–Stokes equations, Numer. Algorithms 42 (2006) 107–126.
[79] Y. Deng, Z. Liu, P. Zhang, Y. Wu, Y. Liu, Topology optimization of steady and unsteady incompressible Navier–Stokes flows driven by body forces, Struct. Multidiscip. Optim. 47 (2013) 555–570.
[80] D.M. Nosenchuck, G.L. Brown, Discrete spatial control of wall shear stress in a turbulent boundary layer, in: Proceedings of the International Conference on Near Wall Turbulence, 1993.
[81] C. Foias, R. Temam, Remarques sur les equations de Navier–Stokes stationnaires et les phenomenes successifs de bifurcation, Ann. Sc. Norm. Super. Pisa (1978) 29–63.
[82] M.D. Gunzburger, L. Hou, T.P. Svobodny, Boundary velocity control of incompressible flow with an application to viscous drag reduction, SIAM J. Control Optim. 30 (1992) 167–181.
[83] S.S. Biringen, Active control of transition by periodic suction-blowing, Phys. Fluids 27 (1984) 1345–1347.
[84] H.O. Fattorini, S.S. Biringen, Existence of optimal controls for viscous flow problems, Proc. R. Soc. Lond. Ser. A 439 (1992) 81–102.
[85] S. Kreissl, G. Pingen, K. Maute, Topology optimization for unsteady flow, Int. J. Numer. Methods Eng. 87 (2011) 1229–1253.